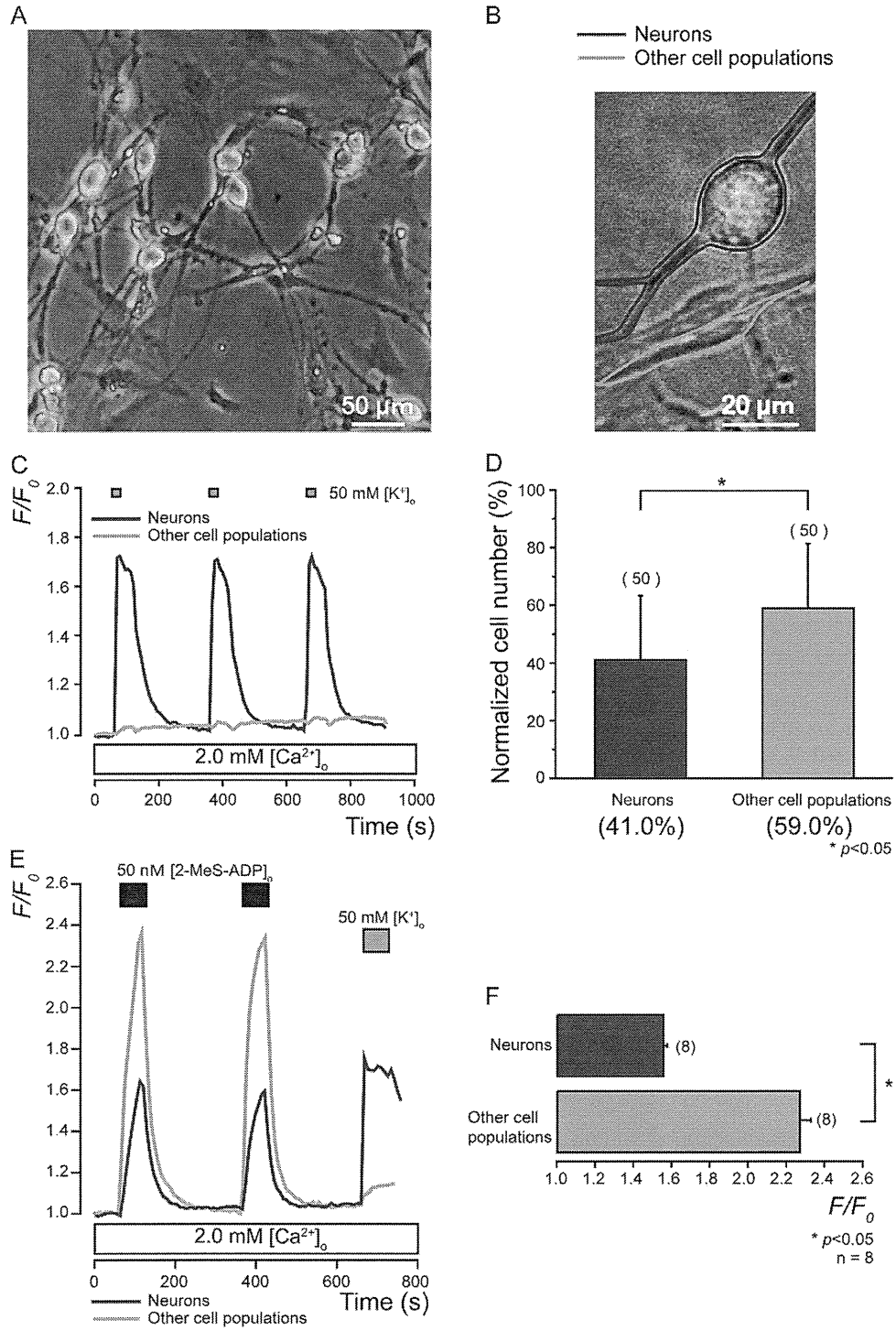

Fig. 1. Characterization of primary cultured TG cells from neonatal Wistar rats. (A) Phase-contrast image shows primary cultures of TG cells. Cells were cultured for 48 h and contained neurons, glial cells, and fibroblasts; scale bar: 50 μm. (B) Image of high magnification shows neurons (red) eliciting depolarization-induced $[Ca^{2+}]_i$ increases and other cell populations (orange). Scale bar: 20 μm. (C) In the presence of 2.0 mM extracellular Ca^{2+} (lower white box), application of 50 mM KCl solution (upper gray boxes) increased $[Ca^{2+}]_i$, indicating that the recorded cells were TG neurons (red solid line in B and C). In contrast, depolarization-induced $[Ca^{2+}]_i$ increases were not observed in some cell populations (orange solid line in B and C). (D) Summary bar graph displays the normalized number of cells tested and the presence or absence of depolarization-induced $[Ca^{2+}]_i$ increases. The percentage of cells responding to the application of a 50-mM KCl solution was 41.0% (red column; neurons), and these cells formed a neuronal cell population. Other cell populations (orange column; 59.0%) did not respond to 50 mM K^+. Data represent the mean ± S.D. of the indicated number of independent experiments (in parentheses). (E) In the presence of 2.0 mM extracellular Ca^{2+} (lower white box), application of 50 nM 2-MeS-ADP (upper black boxes) increased $[Ca^{2+}]_i$ in TG neurons that elicited depolarization-induced $[Ca^{2+}]_i$ increases (red solid line), and other cell populations (orange solid line). Gray box indicates the application of the 50 mM KCl solution. (F) Summary bar graph of $[Ca^{2+}]_i$ increases following the application of 50 nM 2-MeS-ADP in neurons (red column) and other cell populations (orange column). Each column denotes the mean ± S.E. of the indicated number of independent experiments (in parentheses). The statistical significance between columns (shown by solid lines) is indicated by asterisks: $^*p < 0.05$.

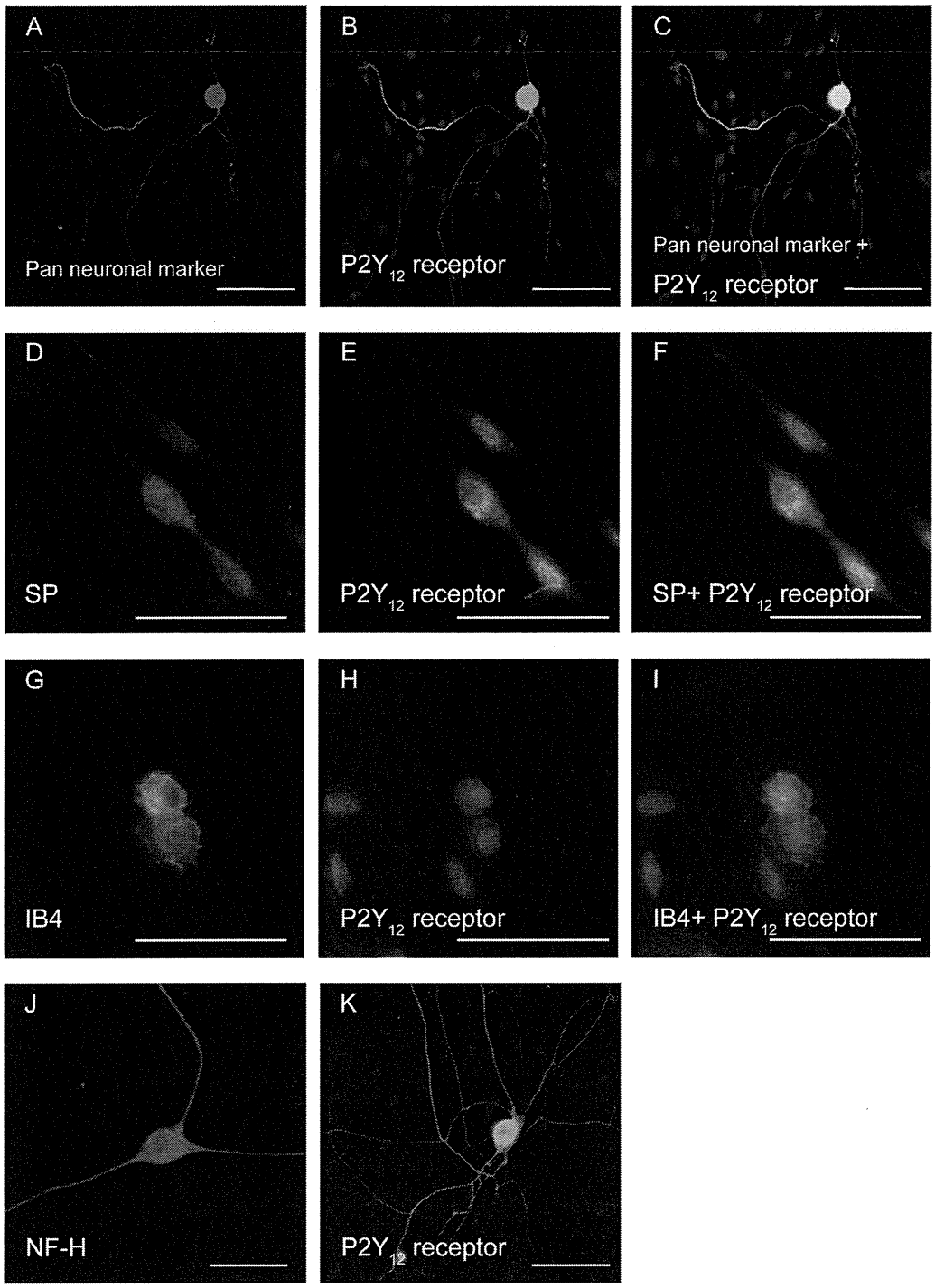

Fig. 2. Immunolocalization of $P2Y_{12}$ receptors in primary cultured TG neurons. (A) Primary cultured TG neurons positive for the pan-neuronal marker. (B, E, H and K) $P2Y_{12}$ receptor immunoreactivity. (C) Triple immunofluorescence staining with antibodies against $P2Y_{12}$ receptors (green) and pan-neuronal marker (red). Nuclei are shown in blue. (D) Positive immunoreactivity to SP as a peptidergic C-neuron marker in primary cultured TG neurons. (F) Triple staining with antibodies against $P2Y_{12}$ receptors (green) and SP (red). Nuclei are shown in blue. (G) Positive immunoreactivity to IB4 as a non-peptidergic C-neuron marker in primary cultured TG neurons. (I) Triple staining with antibodies against $P2Y_{12}$ receptors (red) and IB4 (green). Nuclei are shown in blue. (J) Positive immunoreactivity to NF-H as an A-neuron marker in primary cultured TG neurons. NF-H positive cells exhibited large soma with axons spreading in multiple directions. (K) Neurons of the morphology shown in (J) were also positive for $P2Y_{12}$ receptor immunoreactivity (green). No fluorescence was detected in the negative control (data not shown). Scale bars: 50 μm.

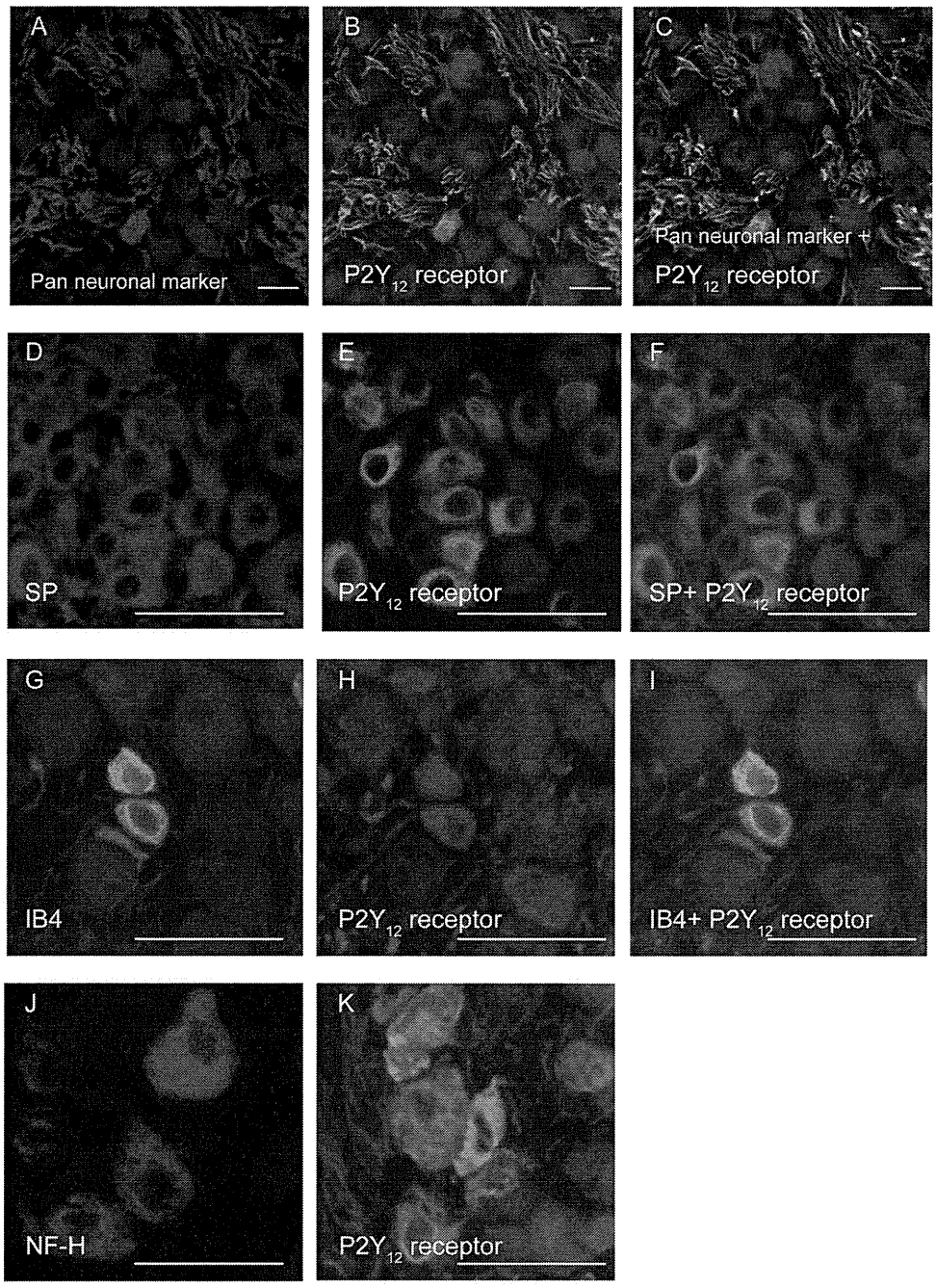

Fig. 3. Immunolocalization of $P2Y_{12}$ receptors in the soma of TG neuron cryosections. (A) TG neurons positive for the pan-neuronal marker. (B, E, H and K) $P2Y_{12}$ receptor immunoreactivity. (C) Triple immunofluorescence staining with antibodies against $P2Y_{12}$ receptors (green) and pan-neuronal marker (red). Nuclei are shown in blue. (D) Positive immunoreactivity to SP as a peptidergic C-neuron marker in TG neurons. (F) Triple staining with antibodies against $P2Y_{12}$ receptors (green) and SP (red). Nuclei are shown in blue. (G) Positive immunoreactivity to IB4 as a non-peptidergic C-neuron marker in TG neurons. (I) Triple staining with antibodies against $P2Y_{12}$ receptors (red) and IB4 (green). Nuclei are shown in blue. (J) Positive immunoreactivity to NF-H as an A-neuron marker in TG neurons. Colocalization of $P2Y_{12}$ receptor and NF-H immunoreactivity could not be examined because both proteins were produced from the same host. No fluorescence was detected in the negative control (data not shown). Scale bars: 20 μm.

The influence of each pharmacological agent on the changes in $[Ca^{2+}]_i$ was analyzed using Origin 8.5 (OriginLab Corporation, Northampton, MA, USA) by fitting the data to the following function using a single-binding model (Eq. (1)):

$$\frac{F}{F_0} = \frac{(F/F_{0\text{int}} - F/F_{0\text{fin}})}{(1 + ([x]_o/K)} + \frac{F}{F_{0\text{fin}}} \quad (1)$$

where K is the equilibrium binding constant, $[x]_o$ indicates the applied concentration of pharmacological agents, and $F/F_{0\text{int}}$ and $F/F_{0\text{fin}}$ are the initial and final F/F_0 responses, respectively.

3. Results

3.1. Characterization of cultured TG neurons

In brightfield image of the primary cultured rat TG cells (Fig. 1A), it was difficult to distinguish the neurons from the SGCs. In order to specifically reveal the neuronal responses, $[Ca^{2+}]_i$ in fura-2-loaded primary cultured TG cells was measured by the application of a solution containing a high concentration of K^+ (50 mM K^+), which induces membrane depolarization. A series of applications

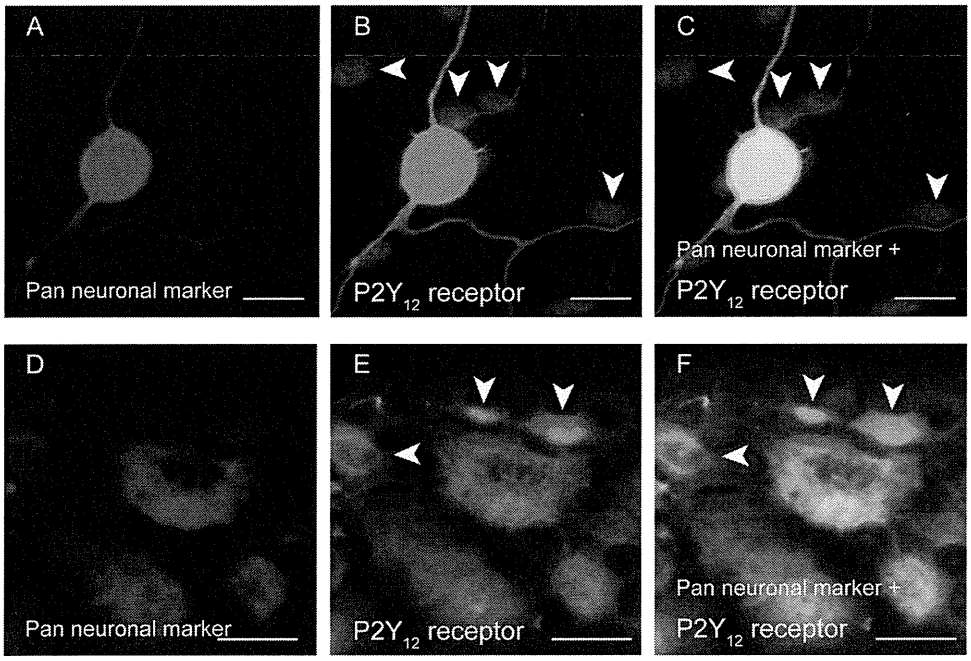

Fig. 4. Neuron marker-negative TG cells exhibited $P2Y_{12}$ receptor immunoreactivity. (A) Primary cultured TG neurons positive for the pan-neuronal marker. (B) $P2Y_{12}$ receptor immunoreactivity was observed in both pan-neuronal marker-positive and pan-neuronal marker-negative cells (arrow heads). (C) Triple immunofluorescence staining with antibodies against $P2Y_{12}$ receptors (green) and pan-neuronal marker (red). Nuclei are shown in blue. (D) Neurons in a TG cryosection positive for the pan-neuronal marker. (E) $P2Y_{12}$ receptor immunoreactivity was observed in both pan-neuronal marker-positive and pan-neuronal marker-negative cells (arrow heads). (F) Triple immunofluorescence staining with antibodies against $P2Y_{12}$ receptors (green) and the pan-neuronal marker (red). Nuclei are shown in blue. Scale bars: 20 μm. Notably, the existence of $P2Y_{12}$ receptor-expressing neuron marker-negative TG cells confirms the specificity of the $P2Y_{12}$ receptor antibody, as a positive control for the results shown in Figs. 2 and 3, because expression of the $P2Y_{12}$ receptor in glial cells has been widely reported (see text).

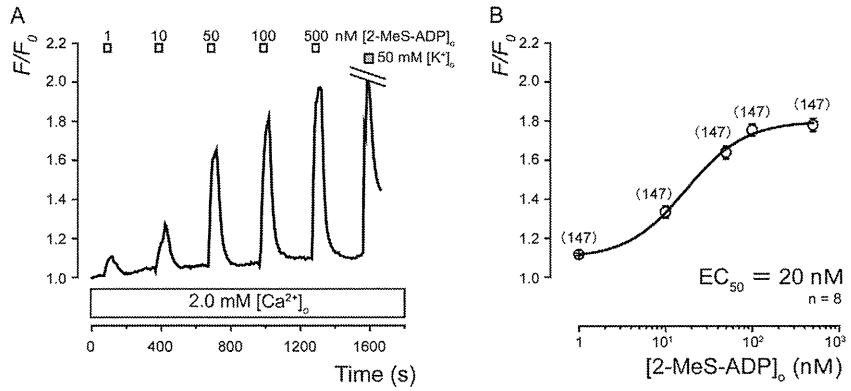

Fig. 5. 2-MeS-ADP induces changes in $[Ca^{2+}]_i$ in the TG neurons. (A) Example of transient increases in $[Ca^{2+}]_i$ following the application of a series of concentrations of 2-MeS-ADP (1–500 nM; upper white boxes) in the presence of extracellular Ca^{2+} (2.0 mM). Application of a 50 mM KCl solution is shown by a gray box. (B) The data points illustrate the F/F_0 values as a function of the applied concentration of 2-MeS-ADP. Each data point represents mean ± S.E. of eight independent experiments (numbers in parentheses represent the number of cells tested). The curve on the semilogarithmic scale was fitted according to Eq. (1) described in the text. The equilibrium binding constant for 2-MeS-ADP was 20 nM. Notably, the dose-dependent relationship between 2-MeS-ADP and $[Ca^{2+}]_i$ increases displayed a good fit to the function when using the single-binding model (Eq. (1)).

of the high K^+ solution induced transient increases in $[Ca^{2+}]_i$ in 41.0% of the tested cultured TG cells (red lines and bar), while the other 59.0% of the TG cells showed no response (orange lines and bar) (Fig. 1B–D). The cells showing $[Ca^{2+}]_i$ increases induced by depolarization were identified as TG neurons (red line in Fig. 1B). Application of 2-MeS-ADP produced a rise in $[Ca^{2+}]_i$, not only in neurons exhibiting depolarization-induced $[Ca^{2+}]_i$ increases (red in Fig. 1E), but also in other cell populations that showed no response to the high K^+ solution (orange in Fig. 1E). The peak increase in $[Ca^{2+}]_i$ elicited by 2-MeS-ADP was 1.5 ± 0.02 F/F_0 units in TG neurons and 2.2 ± 0.7 F/F_0 units in other cell populations, i.e., SGCs. The $[Ca^{2+}]_i$ increases in satellite glial cells (SGCs) were significantly greater than those in neurons (Fig. 1F). Thus, in the present study, a 50-mM K^+ extracellular solution was applied at the end of each experiment to confirm that results were obtained from a pure population of TG neurons.

3.2. Immunolocalization of $P2Y_{12}$ receptors in the TG neurons

The cultured TG neurons showed positive immunoreactivity to a neuronal marker cocktail (Neuro-Chrom™ pan-neuronal marker), which contained mouse anti-NeuN, anti-MAP2, and anti-βIII tubulin antibodies (Fig. 2A; see also Fig. 4A). Positive immunoreactivity was also observed to either substance P (SP; as a peptidergic C-neuron marker; Fig. 2D) or isolectin B4 (IB4; as a non-peptidergic C-neuron marker; Fig. 2G). Intense $P2Y_{12}$

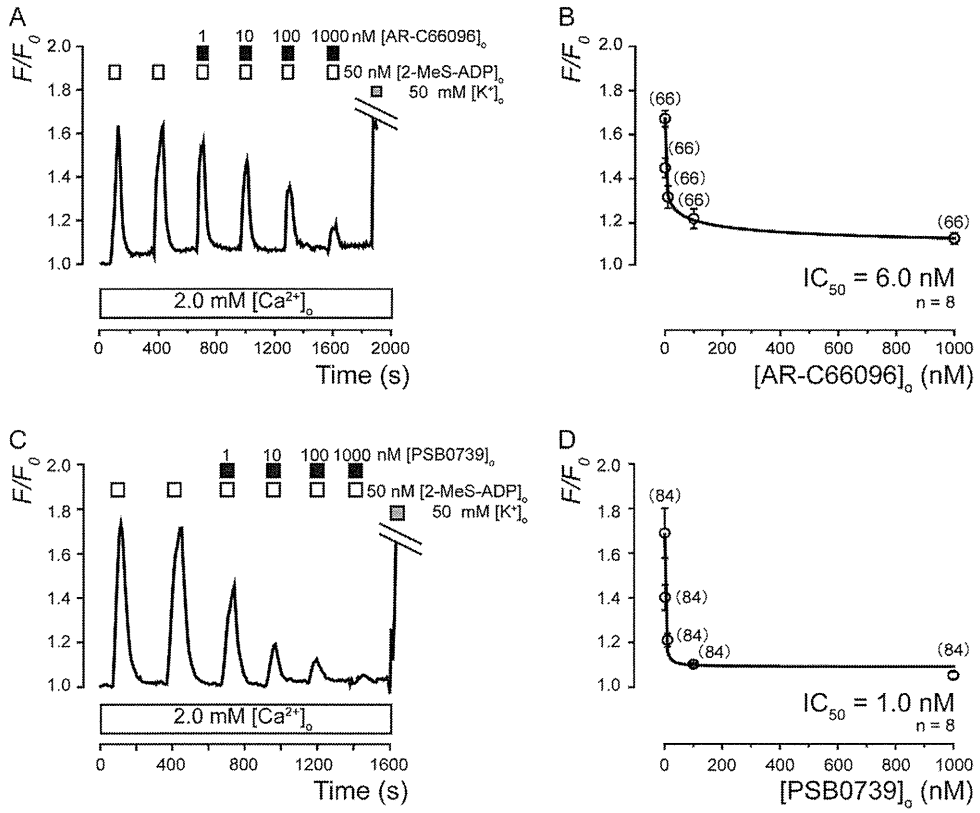

Fig. 6. Pharmacological identification of $P2Y_{12}$ receptors in the TG neurons. (A and C) Dose-dependent inhibitory effect of the selective $P2Y_{12}$ receptors antagonists AR-C66096 (A) and PSB0739 (C), on increases in $[Ca^{2+}]_i$ induced by 2-MeS-ADP in the TG neurons. Example of transient increases in $[Ca^{2+}]_i$ by 50 nM 2-MeS-ADP (upper white boxes), with (black boxes) or without various concentrations of AR-C66096 (1–1000 nM; A) and PSB0739 (1–1000 nM; C), in the presence of extracellular Ca^{2+} (2.0 mM). Times of application of the 50 mM KCl solution are shown in gray boxes. (B and D) Dose-response relations for the inhibitory effects of AR-C66096 (B) and PSB0739 (D) on the increases in $[Ca^{2+}]_i$ induced by 2-MeS-ADP. The data points in each figure illustrate F/F_0 values as a function of the applied concentration of the inhibitors, and represent the mean ± S.E. of eight experiments (numbers in parentheses represent the number of cells tested). The curve on the semilogarithmic scale was fitted according to Eq. (1) described in the text. Notably, the relationship between the dose of $P2Y_{12}$ receptor antagonists (AR-C66096 and PSB0739) and 2-MeS-ADP-induced $[Ca^{2+}]_i$ increases was a good fit to the function using a single-binding model (Eq. (1)).

receptor immunoreactivity was present in the soma, dendrites, and axons, as well as in the perinuclear region of primary cultured TG cells (Figs. 2B, E, H, K and 4B). These $P2Y_{12}$ receptor immunoreactivities colocalized with neurons positive for the pan-neuronal marker (Fig. 2C), SP (Fig. 2F), and IB4 (Fig. 2I). In addition, positive immunoreactivity was observed to NF-H (an A-neuron marker; Fig. 2J), and to the $P2Y_{12}$ receptor in cells that morphologically resembled NF-H-positive TG neurons (Fig. 2K).

In cryosections, TG neurons showed positive immunoreactivity to the pan-neuronal marker (Fig. 3A), SP (Fig. 3D), IB4 (Fig. 3G), and NF-H (Fig. 3J). We also observed intense $P2Y_{12}$ receptor immunoreactivity in the TG cell bodies (Fig. 3B, E, H, and K). These $P2Y_{12}$ receptor immunoreactivities colocalized with neurons positive for the pan-neuronal marker (Fig. 3C), SP (Fig. 3F), and IB4 (Fig. 3I). Notably, NF-H and $P2Y_{12}$ receptor antibodies were produced from the same host. Both NF-H and $P2Y_{12}$ receptor immunoreactivity was identified in TG neurons (Fig. 3J and K).

In cultured cells (Fig. 4A–C) and cryosections (Fig. 4D–F), positive immunoreactivity to the $P2Y_{12}$ receptor was visible in pan-neuronal marker-positive neurons (Fig. 4) and pan-neuronal marker-negative non-neuronal cells (arrowheads in Fig. 4B, C, E, and F).

3.3. 2-MeS-ADP increases $[Ca^{2+}]_i$ in cultured TG neurons

We analyzed the changes in $[Ca^{2+}]_i$ during the application of 2-MeS-ADP, which is a $P2Y_{1,12,13}$ receptor agonist. In the presence of extracellular Ca^{2+} (2.0 mM), addition of five different concentrations of 2-MeS-ADP (1, 10, 50, 100, and 500 nM) induced rapid and transient increases in $[Ca^{2+}]_i$, in a concentration-dependent manner (Fig. 5A). A semilogarithmic plot (Fig. 5B) illustrates F/F_0 values as a function of the applied concentration of 2-MeS-ADP, with an equilibrium-binding constant of 20 nM.

3.4. $P2Y_{12}$-selective antagonists inhibit 2-MeS-ADP-induced increases in the $[Ca^{2+}]_i$ in the TG neurons

In the presence of 2.0 mM extracellular Ca^{2+}, the increases in $[Ca^{2+}]_i$ induced by 2-MeS-ADP were inhibited by various concentrations of the selective $P2Y_{12}$ receptor antagonists AR-C66096 (Fig. 6A) and PSB0739 (Fig. 6C), in a dose-dependent manner. The equilibrium binding constants, represented as the half maximal inhibitory concentrations (IC_{50}), were obtained at an AR-C66096 concentration of 6.0 nM (Fig. 6B) and a PSB0739 concentration of 1.0 nM (Fig. 6D).

3.5. Effects of inhibitors of the ryanodine receptor/channel and SERCA on $[Ca^{2+}]_i$ in TG neurons

In the presence of extracellular Ca^{2+} (2.0 mM), the application of 2-MeS-ADP (50 nM) evoked transient increases in $[Ca^{2+}]_i$ (Fig. 7A–D) to peak values of 1.7 ± 0.06 F/F_0 units in the first application, and 1.6 ± 0.06 F/F_0 units in the second application (Fig. 7D). After completely removing Ca^{2+} from the extracellular solution, the repeated addition of 2-MeS-ADP (50 nM) also produced rapid and transient increases in $[Ca^{2+}]_i$ (Fig. 7A), reaching a peak value

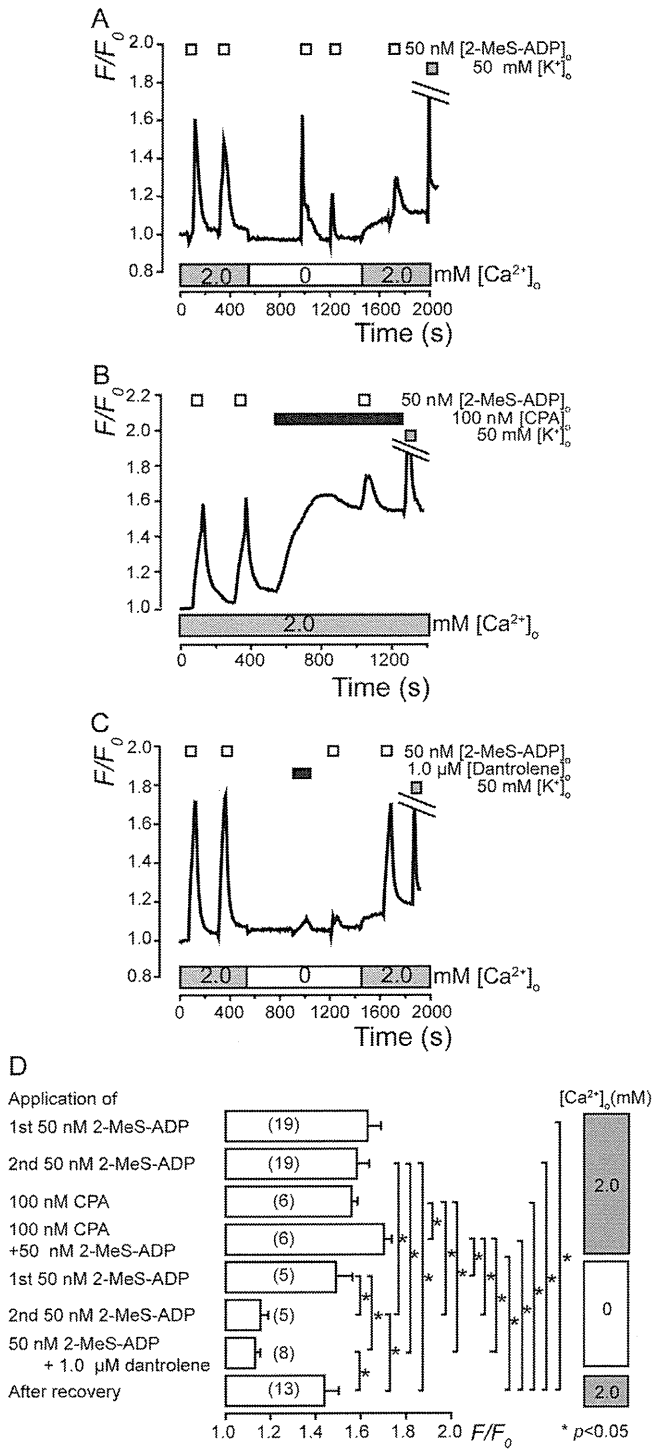

Fig. 7. Effects of ryanodine receptor/channel and sarcoplasmic reticulum Ca^{2+}-ATPase inhibitors on $[Ca^{2+}]_i$.

(A) Example of transient increases in $[Ca^{2+}]_i$ following the application of 50 nM 2-MeS-ADP, with (lower gray boxes) or without (lower white box), extracellular Ca^{2+} (2.0 mM). (B) In the presence of external Ca^{2+}, additions of 50-nM 2-MeS-ADP increased $[Ca^{2+}]_i$. Application of 100 nM of a sarcoplasmic reticulum Ca^{2+}-ATPase (SERCA) inhibitor (cyclopiazonic acid; CPA) gradually elicited an increase in $[Ca^{2+}]_i$, and subsequent application of 2-MeS-ADP (50 nM) induced a further transient $[Ca^{2+}]_i$ increase. (C) The increase in $[Ca^{2+}]_i$ induced by 50 nM 2-MeS-ADP was inhibited by the application of a 1.0 μM dantrolene in the absence of external Ca^{2+}. (A–C) Upper white and black boxes indicate the timing of application of 2-MeS-ADP and the other inhibitors (CPA and dantrolene), respectively. Upper gray boxes indicate the application of the 50 mM KCl solution. (D) Summary bar graph shows increases in $[Ca^{2+}]_i$ following the first (upper column) and second (second column from upper) application of 50 nM 2-MeS-ADP, as well as the application of 100 nM CPA without (third column from upper) and with (fourth column from upper) 50 nM 2-MeS-ADP in the presence of external Ca^{2+} (2.0 mM) (gray boxes on the right side). F/F_0 values after first (fifth column from top) and second (sixth column from top) application of 50 nM 2-MeS-ADP, as well as application of 50 nM 2-MeS-ADP with 1.0 μM dantrolene (seventh column from top) in the absence of external Ca^{2+} (white box on the right side) are shown. After-recovery effect is shown in the eighth column from the top. Each column denotes the mean ± S.E. of the indicated number of independent experiments (in parentheses). Statistical significance between columns (shown by solid lines) is indicated by asterisks: $^*p < 0.05$.

of 1.5 ± 0.07 F/F_0 units in the first application, while the peak value in the second application was significantly lower (Fig. 7A and D). Application of the SERCA inhibitor CPA (100 nM) gradually increased $[Ca^{2+}]_i$ to a value of 1.6 ± 0.03 F/F_0 units (Fig. 7B and D). After the CPA-induced $[Ca^{2+}]_i$ increase had reached a plateau, subsequent application of 2-MeS-ADP resulted in a rapid and transient, but additive increase in $[Ca^{2+}]_i$ (Fig. 7B and D). Preincubation of TG neurons with a ryanodine receptor/channel inhibitor (1.0 μM dantrolene sodium salt; dantrolene), in the absence of external Ca^{2+}, significantly and almost completely abolished 2-MeS-ADP-induced $[Ca^{2+}]_i$ increases to an F/F_0 value of 1.1 ± 0.02 (Fig. 7C and D).

3.6. The increase in $[Ca^{2+}]_i$ induced by the activation of $P2Y_{1,12,13}$ receptors is mediated by a decrease in intracellular cAMP

To elucidate the intracellular signaling pathway mediated by the activation of the $P2Y_{12}$ receptor in the TG neurons, we examined the effects of the adenylate cyclase inhibitor SQ22536, and the phosphodiesterase inhibitor IBMX. Application of five different concentrations (0.01, 0.1, 1.0, 10, 100 μM) of SQ22536 elicited rapid and transient increases in $[Ca^{2+}]_i$, in a concentration-dependent manner (Fig. 8A). A semilogarithmic plot (Fig. 8B) illustrates the F/F_0 values as a function of the applied SQ22536 concentrations, with an EC_{50} of 0.08 μM. In the presence of extracellular Ca^{2+}, 50 μM IBMX significantly and reversibly inhibited the increases in $[Ca^{2+}]_i$ induced by 2-MeS-ADP (1.4 ± 0.05 F/F_0 units) (Fig. 8C and D).

4. Discussion

Previous work has shown that the mRNA of all the P2Y receptor subtypes ($P2Y_1$, $P2Y_2$, $P2Y_4$, $P2Y_6$, $P2Y_{11}$ to $P2Y_{14}$) is expressed in murine TG neurons (Villa et al., 2010b). However, in rat TG neurons, RT-PCR analysis revealed the mRNA expression of only $P2Y_1$, $P2Y_2$, $P2Y_4$, and $P2Y_6$ receptors (Li et al., 2014; Ruan and Burnstock, 2003). The present results clearly indicate that $P2Y_{12}$ receptors are functionally expressed in rat TG neurons, with localization to the soma, axons, and dendrites in A-neurons, non-peptidergic C-neurons, and peptidergic C-neurons. The activation of not only $P2Y_1$ and $P2Y_{13}$, but also $P2Y_{12}$ receptors, elicited mobilization of intracellular Ca^{2+} in the TG neurons. Although only 40% of the primary TG cells showed depolarization-induced increases in $[Ca^{2+}]_i$, all the Ca^{2+} responses in this study were analyzed using cells that exhibited $[Ca^{2+}]_i$ increases on depolarization, which indicates that the data were obtained from neurons, not glial cells.

To examine Ca^{2+} signaling following the activation of the $P2Y_{12}$ receptor, we utilized 2-MeS-ADP as an agonist. In general, there is a consensus on the lack of a selective agonist for the $P2Y_{12}$ receptor. As an agonist, 2-MeS-ADP has been shown to have a high affinity for $P2Y_{1,12,13}$ receptors (Kügelgen, 2008), and has been commonly used to evaluate the functional properties of $P2Y_{12}$ receptors (Bodor et al., 2003; Pausch et al., 2004; Simon et al., 2002). Moreover, recent studies have reported that 2-MeS-ADP acts as a full agonist for the $P2Y_{12}$ receptor by binding to its pocket-like structure; a 2.5 Å structure of $P2Y_{12}$ receptor binds to the full agonist 2-MeS-ADP (Zhang et al., 2014a,b). The $P2Y_{12}$ receptor antagonist AR-C66096

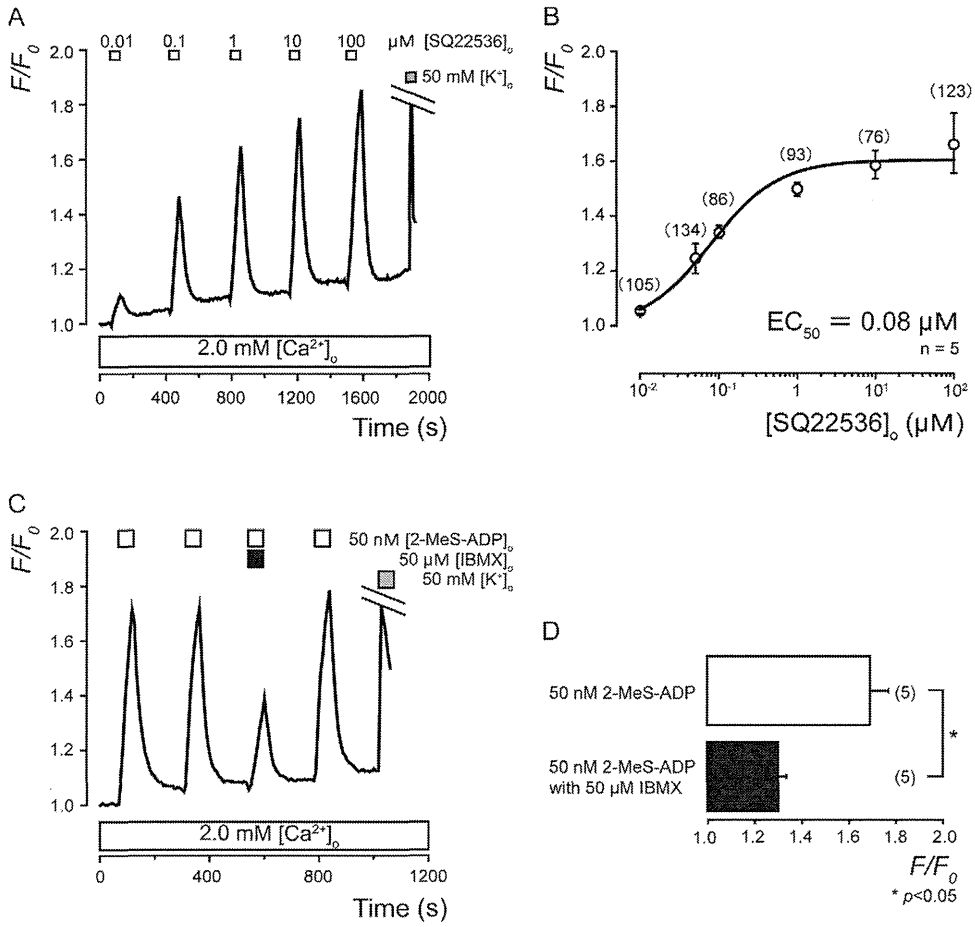

Fig. 8. Intracellular cAMP levels modulate the increases in $[Ca^{2+}]_i$ induced by 2-MeS-ADP in the TG neurons. (A) Example of transient increases in $[Ca^{2+}]_i$ following the application of SQ22536 (0.01–100 μM) (upper white boxes) with external Ca^{2+} (2.0 mM). (B) The data points illustrate F/F_0 values as a function of the applied SQ22536 concentration, and represent the mean ± S.E. of five independent experiments (numbers in parentheses represent the number of cells tested). The curve on the semilogarithmic scale was fitted according to Eq. (1) described in the text, and the equilibrium binding constant of SQ22536 was 0.08 μM. (C) Example of transient increases in $[Ca^{2+}]_i$ during the application of 50 nM 2-MeS-ADP (upper white boxes), with (upper black box), or without 50 μM IBMX, in the presence of external Ca^{2+} (2.0 mM). (D) Summary bar graph of the increases in $[Ca^{2+}]_i$ following the application of 50 nM 2-MeS-ADP, with (bottom black column), or without IBMX (top white column). Each column denotes the mean ± S.E. of the indicated number of independent experiments (in parentheses). Gray boxes indicate the application of the 50 mM KCl solution (A and C). The statistical significance between columns (shown by solid lines), is indicated by asterisks: $*p < 0.05$.

displayed the same binding conformation as that of the $P2Y_{12}$ receptor/2-MeS-ADP complex. In the present study, application of 2-MeS-ADP increased $[Ca^{2+}]_i$, while the selective $P2Y_{12}$ receptor antagonists AR-C66096 and PSB0739 inhibited $[Ca^{2+}]_i$ increases in a dose-dependent manner. In addition, selective antagonists of the $P2Y_{12}$ receptor almost completely abolished the increase in $[Ca^{2+}]_i$ induced by 2-MeS-ADP, making it probable that a major component of the $[Ca^{2+}]_i$ increase was mediated by $P2Y_{12}$ receptor activation.

We also observed that pan-neuronal marker-negative cells, which are located around TG neurons, were positive for $P2Y_{12}$ receptor immunoreactivity and displayed significantly larger 2-MeS-ADP-induced $[Ca^{2+}]_i$ increases compared with neurons. These findings were in accordance with previous studies demonstrating that glial cells in the TG express the $P2Y_{12}$ receptor (Ceruti et al., 2008; Katagiri et al., 2012; Villa et al., 2010a). Although the $P2Y_{12}$ receptor-expressing non-neuronal cells in this study were considered to be glial cells in the TG, Ca^{2+} responses were not further analyzed.

In the present study, the increase in $[Ca^{2+}]_i$ induced by 2-MeS-ADP in TG neurons in the absence of extracellular Ca^{2+} was sensitive to ryanodine receptor/channel inhibitor. Application of the AC inhibitor SQ22536 increased the amplitude of the transient increases in $[Ca^{2+}]_i$ in a concentration-dependent manner, while the phosphodiesterase inhibitor IBMX, significantly and reversibly inhibited the increases in $[Ca^{2+}]_i$ induced by 2-MeS-ADP in TG neurons. These results indicate that the decrease in intracellular cAMP levels, produced by the suppression of AC following the activation of 2-MeS-ADP-sensitive P2Y receptors (including $P2Y_{12}$), increases $[Ca^{2+}]_i$. The activation of $P2Y_{12}$ receptors reduces intracellular cAMP levels in both excitable and non-excitable cells (Kubista et al., 2003; Moskvina et al., 2003; Simon et al., 2002; Unterberger et al., 2002). Furthermore, the decrease in cAMP levels caused by $P2Y_{12}$ receptor activation, and the subsequent increases in $[Ca^{2+}]_i$ are responsible for mediating platelet aggregation (Moheimani and Jackson, 2012).

However, it has been demonstrated that activation of cAMP-dependent protein kinase (protein kinase A; PKA) positively modulates both ryanodine receptors/channels and SERCA on the Ca^{2+} store, to increase $[Ca^{2+}]_i$ and accelerate Ca^{2+} reuptake, respectively (Lymperopoulos et al., 2013). In the present study, a SERCA inhibitor, which inhibits Ca^{2+} reuptake, also elicited gradual $[Ca^{2+}]_i$ increases; however, subsequent application of 2-MeS-ADP produced an additional rapid and transient increase in $[Ca^{2+}]_i$, as shown in Fig. 7. These results indicated that each 2-MeS-ADP-sensitive P2Y receptor activation and each SERCA inhibition acts independently to increase $[Ca^{2+}]_i$. Taken together, our results suggest that P2Y receptor activation in TG neurons decreases intracellular cAMP levels. The reduction in cAMP triggers an increase in

$[Ca^{2+}]_i$ without the contribution of SERCA inhibition. In addition, pre-treatment of TG neurons with dantrolene, a ryanodine receptor/channel inhibitor, suppressed 2-MeS-ADP-induced Ca^{2+} release in TG neurons. Notably, dantrolene also inhibits the ionotropic glutamate receptor (i.e., N-methyl-D-aspartate receptor) (Hayashi et al., 1997; Rossi et al., 2012; Salinska et al., 2008); however, the effect of dantrolene on the 2-MeS-ADP-induced Ca^{2+} release was examined in the absence of extracellular Ca^{2+}, to avoid the contribution of Ca^{2+} influx. Thus, we suggest that the activation of $P2Y_{12}$ receptors induced Ca^{2+} release from intracellular stores via ryanodine receptors/channels, by a decrease in cAMP production via intracellular AC in the TG neurons. Further investigation will be needed to elucidate the detailed mechanism of cAMP-dependent Ca^{2+} release via ryanodine receptors/channels.

Each of the 2-MeS-ADP-sensitive P2Y receptors binds to a single heterotrimeric G protein. The Gq-coupled $P2Y_1$ receptor activates isoforms of the phospholipase C (PLC), leading to the formation of the second messengers 1,2-diacylglycerol and inositol 1,4,5-trisphosphate (IP_3); this mobilizes Ca^{2+} via an IP_3-dependent pathway (Abbracchio et al., 2006). On the other hand, the Gi/o-coupled $P2Y_{12}$ and $P2Y_{13}$ receptors inhibit the AC and activate the phosphoinositide 3-kinase (Gachet et al., 1997; Murugappa and Kunapuli, 2006). $P2Y_{13}$ receptor has also been reported to couple to G $alpha_{16}$ and stimulate PLC (Kim et al., 2005). Although the increase in $[Ca^{2+}]_i$ induced by the Gi protein was associated with AC and cAMP, Gi protein subunits, including the $Gi_{\beta\gamma}$ protein, also activate PLC_β subtypes and $[Ca^{2+}]_i$-increasing pathways via the IP_3 receptor (Bugrim, 1999; Smrcka and Sternweis, 1993). Recently, it has been reported that Gi/o-coupled receptors activate the PLC pathway in dystrophin-deficient mouse muscle cells (Balghi et al., 2006), Chinese hamster ovary cells (Langer and Robberecht, 2005), and human airway smooth muscle cells (Mizuta et al., 2011). A $P2Y_{13}$-like receptor was coupled to PLC stimulation and AC inhibition in rat cerebellar astrocytes (Carrasquero et al., 2005). In the present study, although pre-application of dantrolene almost completely inhibited 2-MeS-ADP-induced Ca^{2+} release in TG neurons, a small residual component of $[Ca^{2+}]_i$ increase was detected during dantrolene application. Thus, the contribution of the PLC signaling cascade to the 2-MeS-ADP-induced Ca^{2+} mobilization in TG neurons could not be excluded; however, Ca^{2+} mobilization by 2-MeS-ADP may be mediated by a cAMP-dependent Gi/o pathway rather than a PLC-coupling Gq pathway.

In conclusion, our results showed that the TG neurons express $P2Y_{12}$ receptors. An agonist for the $P2Y_{12}$ receptor, 2-MeS-ADP, activates $[Ca^{2+}]_i$ increase via activation of intracellular Ca^{2+} releasing pathway through the ryanodine receptors/channels located in the Ca^{2+} store, in cooperation with $P2Y_1$, $P2Y_{12}$ and $P2Y_{13}$ receptors. These pathways that increase $[Ca^{2+}]_i$ are activated by inhibition of intracellular cAMP production, and we suggest that the $P2Y_{12}$ receptor in TG neurons couples with a cAMP-dependent pathway. Gi-coupled P2Y receptors play an important regulatory role in the inhibition of nociceptive signaling (Malin and Molliver, 2010); thus, $P2Y_{12}$ receptors in TG neurons could also be involved in pain signaling in the oral and maxillofacial regions.

Acknowledgement

This research was supported by a Grant-in-Aid for Scientific Research from the Ministry of Education, Culture, Sports, Science, and Technology of Japan (grant #23592751/26861559/25861762).

References

Abbracchio, M.P., Burnstock, G., Boeynaems, J.-M., Barnard, E.A., Boyer, J.L., Kennedy, C., Knight, G.E., Fumagalli, M., Gachet, C., Jacobson, K.A., Weisman, G.A., 2006. International Union of Pharmacology LVIII: update on the P2Y G protein-coupled nucleotide receptors: from molecular mechanisms and pathophysiology to therapy. Pharmacol. Rev. 58, 281–341.

Balghi, H., Sebille, S., Constantin, B., Patri, S., Thoreau, V., Mondin, L., Mok, E., Kitzis, A., Raymond, G., Cognard, C., 2006. Mini-dystrophin expression down-regulates overactivation of G protein-mediated IP3 signaling pathway in dystrophin-deficient muscle cells. J. Gen. Physiol. 127, 171–182.

Basbaum, A.I., Bautista, D.M., Scherrer, G., Julius, D., 2009. Cellular and molecular mechanisms of pain. Cell 139, 267–284.

Bodor, E.T., Waldo, G.L., Hooks, S.B., Corbitt, J., Boyer, J.L., Harden, T.K., 2003. Purification and functional reconstitution of the human $P2Y_{12}$ receptor. Mol. Pharmacol. 64, 1210–1216.

Bugrim, A.E., 1999. Regulation of Ca^{2+} release by cAMP-dependent protein kinase. A mechanism for agonist-specific calcium signaling? Cell Calcium 25, 219–226.

Burnstock, G., 2013. Purinergic signalling: pathophysiology and therapeutic potential. Keio J. Med. 62, 63–73.

Carrasquero, L.M.G., Delicado, E.G., Jiménez, A.I., Pérez-Sen, R., Miras-Portugal, M.T., 2005. Cerebellar astrocytes co-express several ADP receptors. Presence of functional $P2Y_{13}$-like receptors. Purinergic Signal. 1, 153–159.

Ceruti, S., Fumagalli, M., Villa, G., Verderio, C., Abbracchio, M.P., 2008. Purinoceptor-mediated calcium signaling in primary neuron-glia trigeminal cultures. Cell Calcium 43, 576–590.

Cervero, F., Laird, J.M., 1996. Mechanisms of touch-evoked pain (allodynia): a new model. Pain 68, 13–23.

Dussor, G., Koerber, H.R., Oaklander, A.L., Rice, F.L., Molliver, D.C., 2009. Nucleotide signaling and cutaneous mechanisms of pain transduction. Brain Res. Rev. 60, 24–35.

Fried, K., Bongenhielm, U., Boissonade, F.M., Robinson, P.P., 2001. Nerve injury-induced pain in the trigeminal system. Neurosci. Rev. J. Bringing Neurobiol. Neurol. Psychiatry 7, 155–165.

Gachet, C., Hechler, B., Léon, C., Vial, C., Leray, C., Ohlmann, P., Cazenave, J.P., 1997. Activation of ADP receptors and platelet function. Thromb. Haemost. 78, 271–275.

Giachini, F.R., Leite, R., Osmond, D.A., Lima, V.V., Inscho, E.W., Webb, R.C., Tostes, R.C., 2014. Anti-platelet therapy with clopidogrel prevents endothelial dysfunction and vascular remodeling in aortas from hypertensive rats. PLOS ONE 9, e91890.

Hayashi, T., Kagaya, A., Takebayashi, M., Oyamada, T., Inagaki, M., Tawara, Y., Yokota, N., Horiguchi, J., Su, T.P., Yamawaki, S., 1997. Effect of dantrolene on KCl- or NMDA-induced intracellular Ca^{2+} changes and spontaneous Ca^{2+} oscillation in cultured rat frontal cortical neurons. J. Neural Transm. Vienna Austria 1996 (104), 811–824.

Katagiri, A., Shinoda, M., Honda, K., Toyofuku, A., Sessle, B.J., Iwata, K., 2012. Satellite glial cell $P2Y_{12}$ receptor in the trigeminal ganglion is involved in lingual neuropathic pain mechanisms in rats. Mol. Pain 8, 23.

Kim, Y.-C., Lee, J.-S., Sak, K., Marteau, F., Mamedova, L., Boeynaems, J.-M., Jacobson, K.A., 2005. Synthesis of pyridoxal phosphate derivatives with antagonist activity at the $P2Y_{13}$ receptor. Biochem. Pharmacol. 70, 266–274.

Kobayashi, K., Yamanaka, H., Fukuoka, T., Dai, Y., Obata, K., Noguchi, K., 2008. $P2Y_{12}$ receptor upregulation in activated microglia is a gateway of p38 signaling and neuropathic pain. J. Neurosci. Off. J. Soc. Neurosci. 28, 2892–2902.

Kubista, H., Lechner, S.G., Wolf, A.M., Boehm, S., 2003. Attenuation of the P2Y receptor-mediated control of neuronal Ca^{2+} channels in PC12 cells by antithrombotic drugs. Br. J. Pharmacol. 138, 343–350.

von Kügelgen, I., 2008. Pharmacology of Mammalian P2X- and P2Y-Receptors.

Kuroda, H., Sobhan, U., Sato, M., Tsumura, M., Ichinohe, T., Tazaki, M., Shibukawa, Y., 2013. Sodium–calcium exchangers in rat trigeminal ganglion neurons. Mol. Pain 9, 22.

Langer, I., Robberecht, P., 2005. Mutations in the carboxy-terminus of the third intracellular loop of the human recombinant $VPAC_1$ receptor impair VIP-stimulated $[Ca^{2+}]_i$ increase but not adenylate cyclase stimulation. Cell. Signal. 17, 17–24.

Li, N., Lu, Z., Yu, L., Burnstock, G., Deng, X., Ma, B., 2014. Inhibition of G protein-coupled $P2Y_2$ receptor induced analgesia in a rat model of trigeminal neuropathic pain. Mol. Pain 10, 21.

Lymperopoulos, A., Rengo, G., Koch, W.J., 2013. Adrenergic nervous system in heart failure pathophysiology and therapy. Circ. Res. 113, 739–753.

Malin, S.A., Molliver, D.C., 2010. Gi- and Gq-coupled ADP (P2Y) receptors act in opposition to modulate nociceptive signaling and inflammatory pain behavior. Mol. Pain 6, 21.

Mizuta, K., Mizuta, F., Xu, D., Masaki, E., Panettieri, R.A., Emala, C.W., 2011. Gi-coupled γ-aminobutyric acid-B receptors cross-regulate phospholipase C and calcium in airway smooth muscle. Am. J. Respir. Cell Mol. Biol. 45, 1232–1238.

Moheimani, F., Jackson, D.E., 2012. $P2Y_{12}$ receptor: platelet thrombus formation and medical interventions. Int. J. Hematol. 96, 572–587.

Moskvina, E., Unterberger, U., Boehm, S., 2003. Activity-dependent autocrine–paracrine activation of neuronal P2Y receptors. J. Neurosci. Off. J. Soc. Neurosci. 23, 7479–7488.

Murugappa, S., Kunapuli, S.P., 2006. The role of ADP receptors in platelet function. Front. Biosci. J. Virtual Libr. 11, 1977–1986.

Ochoa, J.L., 2009. Neuropathic pain: redefinition and a grading system for clinical and research purposes. Neurology 72, 1282–1283.

Pausch, M.H., Lai, M., Tseng, E., Paulsen, J., Bates, B., Kwak, S., 2004. Functional expression of human and mouse $P2Y_{12}$ receptors in *Saccharomyces cerevisiae*. Biochem. Biophys. Res. Commun. 324, 171–177.

Pinheiro, A.R., Paramos-de-Carvalho, D., Certal, M., Costa, C., Magalhães-Cardoso, M.T., Ferreirinha, F., Costa, M.A., Correia-de-Sá, P., 2013. Bradykinin-induced Ca^{2+} signaling in human subcutaneous fibroblasts involves ATP release via hemichannels leading to $P2Y_{12}$ receptors activation. Cell Commun. Signal. CCS 11, 70.

Rossi, B., Ogden, D., Llano, I., Tan, Y.P., Marty, A., Collin, T., 2012. Current and calcium responses to local activation of axonal NMDA receptors in developing cerebellar molecular layer interneurons. PLoS ONE 7, e39983.

Ruan, H.Z., Burnstock, G., 2003. Localisation of $P2Y_1$ and $P2Y_4$ receptors in dorsal root, nodose and trigeminal ganglia of the rat. Histochem. Cell Biol. 120, 415–426.

Salinska, E., Sobczuk, A., Lazarewicz, J.W., 2008. Dantrolene antagonizes the glycine B site of the NMDA receptor. Neurosci. Lett. 432, 137–140.

Scholz, J., Woolf, C.J., 2002. Can we conquer pain? Nat. Neurosci. 5 (Suppl.), 1062–1067.

Simon, J., Filippov, A.K., Göransson, S., Wong, Y.H., Frelin, C., Michel, A.D., Brown, D.A., Barnard, E.A., 2002. Characterization and channel coupling of the $P2Y_{12}$ nucleotide receptor of brain capillary endothelial cells. J. Biol. Chem. 277, 31390–31400.

Smrcka, A.V., Sternweis, P.C., 1993. Regulation of purified subtypes of phosphatidylinositol-specific phospholipase C beta by G protein alpha and beta gamma subunits. J. Biol. Chem. 268, 9667–9674.

Tozaki-Saitoh, H., Tsuda, M., Miyata, H., Ueda, K., Kohsaka, S., Inoue, K., 2008. $P2Y_{12}$ receptors in spinal microglia are required for neuropathic pain after peripheral nerve injury. J. Neurosci. 28, 4949–4956.

Unterberger, U., Moskvina, E., Scholze, T., Freissmuth, M., Boehm, S., 2002. Inhibition of adenylyl cyclase by neuronal P2Y receptors. Br. J. Pharmacol. 135, 673–684.

Villa, G., Ceruti, S., Zanardelli, M., Magni, G., Jasmin, L., Ohara, P.T., Abbracchio, M.P., 2010a. Temporomandibular joint inflammation activates glial and immune cells in both the trigeminal ganglia and in the spinal trigeminal nucleus. Mol. Pain 6, 89.

Villa, G., Fumagalli, M., Verderio, C., Abbracchio, M.P., Ceruti, S., 2010b. Expression and contribution of satellite glial cells purinoceptors to pain transmission in sensory ganglia: an update. Neuron Glia Biol. 6, 31–42.

Zhang, J., Zhang, K., Gao, Z.-G., Paoletta, S., Zhang, D., Han, G.W., Li, T., Ma, L., Zhang, W., Müller, C.E., Yang, H., Jiang, H., Cherezov, V., Katritch, V., Jacobson, K.A., Stevens, R.C., Wu, B., Zhao, Q., 2014a. Agonist-bound structure of the human $P2Y_{12}$ receptor. Nature 509, 119–122.

Zhang, K., Zhang, J., Gao, Z.-G., Zhang, D., Zhu, L., Han, G.W., Moss, S.M., Paoletta, S., Kiselev, E., Lu, W., Fenalti, G., Zhang, W., Müller, C.E., Yang, H., Jiang, H., Cherezov, V., Katritch, V., Jacobson, K.A., Stevens, R.C., Wu, B., Zhao, Q., 2014b. Structure of the human $P2Y_{12}$ receptor in complex with an antithrombotic drug. Nature 509, 115–118.

Effects of Volatile Anesthetics on Oral Tissue Blood Flow in Rabbits: A Comparison Among Isoflurane, Sevoflurane, and Desflurane

*Sota Okamoto, DDS, PhD, *Nobuyuki Matsuura, DDS, PhD, † and Tatsuya Ichinohe, DDS, PhD‡*

Purpose: The aim of this study was to compare the concentration-dependent effects of isoflurane, sevoflurane, and desflurane on oral tissue blood flow.

Materials and Methods: Thirty male Japan White rabbits were randomized to receive 1 of 3 volatile anesthetics: isoflurane (group Iso), sevoflurane (group Sevo), or desflurane (group Des). The end-tidal concentration of each volatile anesthetic was regulated to 0.5, 1, and 1.5 minimum alveolar concentrations (MACs). The observed variables were heart rate, systolic blood pressure, diastolic blood pressure, mean arterial pressure, common carotid arterial blood flow, tongue mucosal blood flow, mandibular bone marrow blood flow (BBF), masseter muscle blood flow (MBF), upper alveolar tissue blood flow, and lower alveolar tissue blood flow (LBF).

Results: The blood pressure in each group tended to decrease depending on the concentration of each volatile anesthetic, with the smallest effect in group Des. BBF and MBF in group Iso were higher than those in group Des at 1 MAC, and MBF and LBF in group Iso were highest at 1.5 MAC.

Conclusion: The results of this study suggest that each volatile anesthetic produced unique effects on blood flow in oral tissues and circulatory parameters. Among the 3 volatile anesthetics, desflurane produced the smallest effects on oral tissue blood flow.

J Oral Maxillofac Surg 73:1714.e1-1714.e8, 2015

Volatile anesthetics are commonly used for general anesthesia. They increase cerebral blood flow in a concentration-dependent manner.[1-3] Sevoflurane has been reported to decrease blood flow in the rat coronary artery or renal artery more than isoflurane at 0.7 minimum alveolar concentration (MAC).[4] Isoflurane has been found to exhibit a more potent vasodilatory effect in smaller vessels than in larger vessels in isolated dog coronary arteries.[5] Sevoflurane and desflurane have been found to suppress acetylcholine-induced release of endothelium-derived hyperpolarizing factor and decrease the vasodilatory effect on the rabbit carotid artery.[6] Although these studies have investigated effects in large vessels, there is sparse research investigating the effect of volatile anesthetics on regional tissue blood flow.

Several studies have investigated oral tissue blood flow in rabbits.[7-13] Handa et al[7] compared the effect of arterial carbon dioxide partial pressure on oral tissue blood flow during isoflurane and propofol anesthesia and found that oral tissue blood flow was higher with isoflurane. Sazuka et al[9] investigated the effect of dexmedetomidine on oral tissue blood flow during sevoflurane and propofol anesthesia and found

Received from the Department of Dental Anesthesiology, Tokyo Dental College, Chiba, Japan.

*Postgraduate Student.

†Senior Assistant Professor.

‡Professor and Chairman.

This work was supported in part by JSPS KAKENHI (grant 25463147).

Address correspondence and reprint requests to Dr Okamoto: Department of Dental Anesthesiology, Tokyo Dental College, 1-2-2, Masago, Mihama-ku, Chiba-shi, Chiba, 261-8502, Japan; e-mail: getaniyakimiso@mac.com

Received January 9 2015

Accepted March 16 2015

0278-2391/15/00339-0

http://dx.doi.org/10.1016/j.joms.2015.03.047

Table 1. HEMODYNAMIC VARIABLES AND TISSUE BLOOD FLOW

	Isoflurane			
	Control	0.5 MAC	1.0 MAC	1.5 MAC
SBP (mmHg)	127.9 ± 12.3	117.9 ± 14.4*	102.4 ± 11.7*	85.5 ± 10.4*
DBP (mmHg)	67.7 ± 6.4	57.2 ± 10.2*	47.1 ± 9.6*	37.3 ± 8.2*
MAP (mmHg)	87.6 ± 5.7	83.0 ± 8.9	72.5 ± 10.5*	60.1 ± 7.0*
HR (beats/minute)	269.3 ± 33.6	300.6 ± 26.7*	311.2 ± 23.7*	298.4 ± 15.3*
CCBF (mL/minute)	54.8 ± 11.1	54.5 ± 11.0	55.7 ± 12.4	56.9 ± 11.6
TBF (mL/minute)	41.1 ± 7.4	40.6 ± 6.9	42.5 ± 6.0	52.6 ± 10.1*
BBF (mL • min^{-1} • 100 g^{-1})	35.5 ± 4.1	40.6 ± 6.8*	46.5 ± 4.8*	47.0 ± 6.4*
MBF (mL • min^{-1} • 100 g^{-1})	33.1 ± 4.4	34.7 ± 5.1	44.3 ± 5.2*	47.5 ± 4.8*
UBF (mL • min^{-1} • 100 g^{-1})	28.8 ± 4.6	29.0 ± 4.2	30.9 ± 5.3	34.9 ± 8.5*
LBF (mL • min^{-1} • 100 g^{-1})	39.1 ± 5.0	44.9 ± 5.6	51.8 ± 11.6*	62.2 ± 14.5*

Note: Data are expressed as mean ± standard deviation.
Abbreviations: BBF, bone marrow blood flow; CCBF, common carotid artery blood flow; DBP, diastolic blood pressure; HR, heart rate; LBF, lower alveolar tissue blood flow; MAC, minimum alveolar concentration; MAP, mean arterial pressure; MBF, masseter muscle blood flow; SBP, systolic blood pressure; TBF, tongue mucosal blood flow; UBF, upper alveolar tissue blood flow.
*$P < .05$ versus control.

Okamoto, Matsuura, and Ichinohe. Effects of Anesthetics on Oral Blood Flow. J Oral Maxillofac Surg 2015.

less oral tissue blood flow with sevoflurane. These studies suggest that volatile anesthetics also affect regional tissue blood flow. However, the effects of changes in volatile anesthetic concentrations on oral tissue blood flow have not been adequately clarified.

This study investigated the effects of volatile anesthetics on oral tissue blood flow and systemic circulation and the concentration dependence of these effects. The authors measured circulatory variables during isoflurane, sevoflurane, or desflurane inhalation and assessed changes in common carotid artery blood flow (CCBF), tongue mucosal blood flow (TBF), mandibular bone marrow blood flow (BBF), masseter muscle blood flow (MBF), upper alveolar tissue blood flow (UBF), and lower alveolar tissue blood flow (LBF).

Materials and Methods

The study was approved by the animal experiments committee at Tokyo Dental College (Tokyo, Japan; approval number 252501). Thirty male Japan White rabbits, each weighing approximately 2.5 kg, were used. Anesthesia was induced by inhalation of oxygen and 3.0% isoflurane (Forane, Abbott Japan, Tokyo, Japan) through a mask. After infiltration anesthesia using 0.5 mL of 1% lidocaine hydrochloride (Xylocaine, AstraZeneca, Osaka, Japan), a tracheotomy was performed and a 20-Fr pediatric tracheal tube was inserted and fixed. The right femoral artery was exposed, and an indwelling 20-gauge catheter was inserted. Blood pressure was recorded continuously with a pressure transducer (P231D, Gould, Oxnard, CA). Heart rate (HR) was calculated from the pressure waveform. An indwelling 22-gauge catheter was inserted into the auricular marginal vein and acetated Ringer solution containing 1% glucose was infused at 10 mL/kg per hour. Muscle relaxation was achieved through continuous infusion of rocuronium bromide (Eslax, Schering-Plough, Tokyo, Japan) at 14 μg/kg per minute.[11] Ventilation was controlled at approximately 50 mL per breath and a rate of 30 to 40 breaths/minute, and end-tidal carbon dioxide partial pressure ($ETCO_2$) was maintained at 35 to 40 mmHg. $ETCO_2$ and anesthetic gas concentration were monitored continuously using an anesthetic gas monitor (Capnomac Ultima, Datex, Helsinki, Finland).

The probe (type 3SB) of an ultrasonic blood flowmeter (T108, Transonic, Ithaca, NY) was attached to the left common carotid artery that had been separated from the surrounding tissues. The inferior margin of the left mandible was excised without the use of local anesthetic and the masseter muscle and periosteum of the mandibular body were exposed. The periosteum was detached to expose the bone surface and a round burr (ISO 008, Morita, Saitama, Japan) was used to make a hole in the cortical bone to provide access to the bone marrow. The probe of a hydrogen clearance tissue blood flowmeter (UHE-100, Unique Medical, Tokyo, Japan) was inserted into the left mandibular bone marrow, left masseter muscle, and alveolar mucosal tissue in the left maxilla and mandible on the labial side of the incisors. The probe (type C) of a laser Doppler blood flowmeter (ALF21, Unique Medical) was tightly attached to the dorsal mucosa on the left side of the tongue.

Table 1. CONT'D

Sevoflurane				Desflurane			
Control	0.5 MAC	1.0 MAC	1.5 MAC	Control	0.5 MAC	1.0 MAC	1.5 MAC
123 ± 10.7	121.8 ± 13.1	105.7 ± 17.3*	92.6 ± 15.1*	127 ± 11.3	117.2 ± 15.9*	121.7 ± 15.1	104.6 ± 27.2*
69.4 ± 9.0	62.4 ± 7.6*	49.5 ± 7.5*	42.3 ± 7.0*	69.5 ± 6.5	59.7 ± 11.8	64.8 ± 15.9	49.2 ± 14.8*
93.7 ± 6.9	83.9 ± 5.9*	71.0 ± 10.5*	60.9 ± 6.9*	92.0 ± 5.7	82.9 ± 9.0	88.4 ± 12.5	73.5 ± 14.3*
275.1 ± 32.2	285.3 ± 25.6	293.9 ± 26.8	290.7 ± 24.9	273.7 ± 32.9	273.7 ± 35.3	286.2 ± 36.3	322.3 ± 25.3*
57.4 ± 8.7	52.0 ± 10.5	49.1 ± 12.4	50.1 ± 14.6	54.7 ± 8.2	55.1 ± 9.8	63.6 ± 15.9	60.2 ± 15.6
40.3 ± 4.4	37.1 ± 6.5	36.9 ± 6.9	43.0 ± 10.0	37.5 ± 5.4	38.1 ± 6.7	38.44 ± 6.4	44.8 ± 8.1
37.8 ± 5.0	41.3 ± 4.4	41.5 ± 3.8	41.9 ± 6.3	34.3 ± 6.4	35.4 ± 7.7	38.2 ± 10.3	38.7 ± 11.0
31.0 ± 2.9	35.6 ± 4.8*	39.1 ± 7.9*	39.6 ± 8.5*	31.7 ± 5.1	33.6 ± 7.4	34.6 ± 7.9	35.2 ± 8.6
26.4 ± 3.7	32.2 ± 4.4	28.5 ± 6.0	30.4 ± 6.2	27.2 ± 7.4	29.2 ± 8.3	29.2 ± 9.2	31.2 ± 9.4
37.5 ± 6.5	41.8 ± 6.9	44.5 ± 6.2	47.5 ± 10.4*	36.6 ± 5.0	39.8 ± 6.1	41.9 ± 3.9*	50.3 ± 12.1*

After completing the experimental preparations, isoflurane inhalation was stopped, and propofol (Diprivan, AstraZeneca, Tokyo, Japan) was infused at 12 mg/kg per hour. After the rabbits were left for at least 1 hour until isoflurane could no longer be detected on the breath, the control values were measured.

Then, the animals were randomly allocated using a random-number table to the isoflurane group (group Iso; n = 10), sevoflurane (Sevofrane, Maruishi Pharmaceutical, Osaka, Japan) group (group Sevo; n = 10), or desflurane (Suprane, Baxter, Tokyo, Japan) group (group Des; n = 10). Infusion of propofol was stopped and the end-tidal concentration of each volatile anesthetic was regulated to 0.5, 1, and 1.5 MAC. The authors used MACs of 2.1% for isoflurane, 3.7% for sevoflurane, and 8.9% for desflurane.[14-16] Measurements were performed 60 minutes after the start of inhalation at 0.5 MAC to minimize the hemodynamic effects of propofol and 30 minutes after the start of inhalation at 1.0 or 1.5 MAC. After all observations were completed and volatile anesthetic administration was stopped, the authors confirmed the recovery in tissue blood flow and the parameters for systemic circulation. Once the end-tidal concentration of the volatile anesthetic had decreased to lower than 0.05 MAC (isoflurane, 0.1%; sevoflurane, 0.15%; desflurane, 0.45%), the parameters were measured after 30 minutes and the results were compared with the measurements from before volatile anesthetic administration.

Systolic blood pressure (SBP), diastolic blood pressure (DBP), mean arterial pressure (MAP), HR, CCBF, and TBF were recorded continuously on a polygraph (Series 360, NEC Sanei, Tokyo). BBF, MBF, UBF, and LBF were measured using a hydrogen-clearance tissue blood flowmeter and the data were analyzed using a data collection analysis system (UCO, Unique Medical). Data in this report are expressed as mean ± standard deviation. For CCBF and tissue blood flow values, the percentage of change was calculated, with the control value as 100%. For statistical analysis, repeated measures analysis of variance (ANOVA) was used for comparisons with the control value for each volatile anesthetic at the various MACs and the Dunnett test was used for multiple comparisons. Non-repeated measures ANOVA was used to compare the 3 types of volatile anesthetic and the Student-Newman-Keuls test was used for multiple comparisons. A P value less than .05 was considered statistically significant.

Results

No statistical differences were observed among the control values of the 3 groups before volatile anesthetic administration. Recovery in all parameters was observed after the experiment in the 3 groups and no statistical differences from the control values before the experiment were observed (data not shown).

COMPARISON BETWEEN CONTROL VALUE AND VALUES AT EACH MAC FOR THE SAME VOLATILE ANESTHETIC

Blood pressure decreased as the concentration increased in each group (Table 1, Fig 1). A comparison of MAP at 1.5 MAC and the control value showed

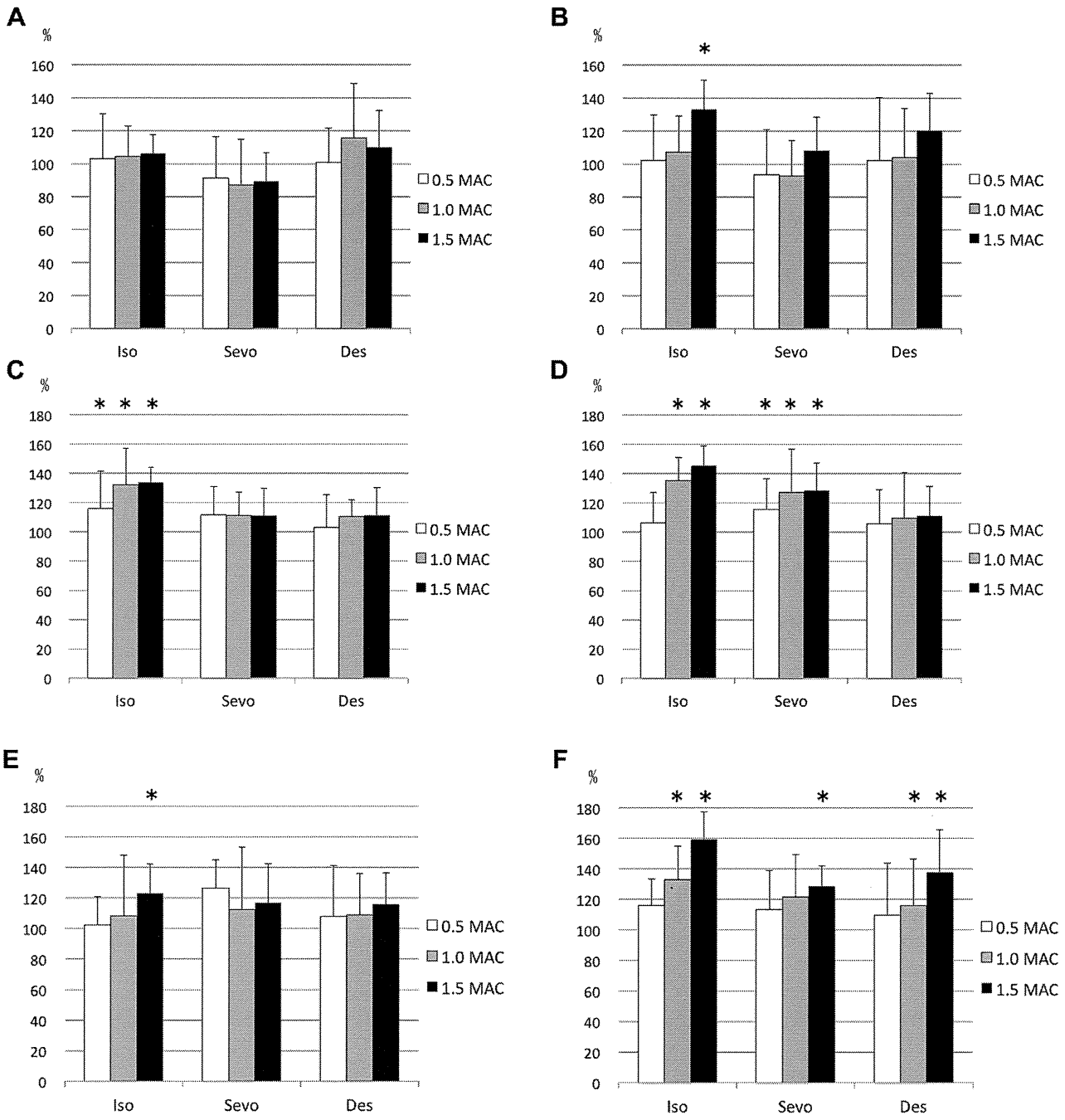

FIGURE 1. Graphs present comparisons of each MAC for the same volatile anesthetics. *A*, Percentage of changes from control in CCBF. *B*, Percentage of changes from control in TBF. *C*, Percentage of changes from control in BBF. *D*, Percentage of changes from control in MBF. *E*, Percentage of changes from control in UBF. *F*, Percentage of changes from control in LBF. *$P < .05$ versus control. BBF, bone marrow blood flow; CCBF, common carotid artery blood flow; DBP, diastolic blood pressure; Des, desflurane; HR, heart rate; Iso, isoflurane; LBF, lower alveolar tissue blood flow; MAC, minimum alveolar concentration; MAP, mean arterial pressure; MBF, masseter muscle blood flow; SBP, systolic blood pressure; Sevo, sevoflurane; TBF, tongue mucosal blood flow; UBF, upper alveolar tissue blood flow.

Okamoto, Matsuura, and Ichinohe. Effects of Anesthetics on Oral Blood Flow. J Oral Maxillofac Surg 2015.

decreases of 31% in group Iso, 35% in group Sevo, and 20% in group Des. HR increased by 13% in group Iso and 20% in group Des. No statistical difference was observed in group Sevo. No statistical change in CCBF was observed in any of the groups. For tissue blood flow in group Iso, BBF increased statistically at 0.5 MAC; BBF, MBF, and UBF increased at 1.0 MAC; and blood flow increased in all tissues when the concentration was increased to 1.5 MAC. In group Sevo, MBF increased at all concentrations and LBF increased at 1.5 MAC. In group Des, LBF increased at 1.0 and 1.5 MAC.

COMPARISON AMONG VOLATILE ANESTHETICS AT THE SAME MAC

No statistical differences were observed at 0.5 MAC for all parameters (Table 1, Fig 2). At 1.0 MAC, SBP, DBP, and MAP were higher in group Des than in groups Iso and Sevo. BBF and MBF in group Iso were higher than those in group Des, whereas LBF in group Iso was higher than that in groups Des and Sevo. At 1.5 MAC, MAP and HR in group Des and MBF and LBF in group Iso showed the highest values.

Discussion

The results from this study showed that each volatile anesthetic had different effects on circulatory parameters, such as blood pressure and HR, and on oral tissue blood flow. At 0.5 MAC, no statistical differences were observed in the parameters among the 3 volatile anesthetics. A concentration-dependent decrease in blood pressure was observed in all groups, although there was only a small change in group Des at 1.0 and 1.5 MAC. As the concentration increased, there was a large increase in HR in group Des and blood flow increased in all oral tissues in group Iso. Importantly, MBF and LBF increased in group Sevo and LBF increased in group Des, although the percentage of change in these parameters was less than in group Iso. In a study by Özarslan et al,[17] the circulatory parameters of blood pressure and HR did not correlate with regional tissue blood flow and they reported that it was difficult to estimate tissue blood flow using these parameters. The present results suggest that these volatile anesthetics have different effects on small vessels in oral peripheral tissues and on circulatory parameters. Therefore, it is difficult to predict the blood flow of oral tissues from circulatory parameters.

In this study, blood pressure decreased as the concentration of each volatile anesthetic increased. Volatile anesthetics have been reported to produce a concentration-dependent decrease in cardiac output.[18] Volatile anesthetics also have been found to exhibit a vasodilatory action.[5,19,20] All volatile anesthetics in the present study could have caused a decrease in cardiac output and vasodilation as the concentration increased, which would have caused blood pressure to decrease. However, the degree of vasodilation differed according to the agent. Sevoflurane has been found to exhibit a smaller vasodilatory effect than isoflurane,[5] and desflurane has been found to produce a smaller vasodilatory effect than sevoflurane.[19] It has been reported that desflurane does not meaningfully affect systemic vascular resistance.[20] These findings explain at least in part why blood pressure in group Des was maintained at 1.0 MAC, and why blood pressure decreased less in group Des as the concentration was increased to 1.5 MAC.

Volatile anesthetics affect the autonomic nervous system and differences in blood pressure or HR are believed to be due to the degree of impact on the autonomic nervous system.[21,22] The degree of increase in HR by volatile anesthetics has been reported to depend on differences in their vagal activity, and desflurane has been found to produce the greatest increase in HR.[23] Desflurane is a structural isomer of isoflurane and has characteristics similar to those of isoflurane.[24] Isoflurane-induced tachycardia has been found to be the result mainly of vagal withdrawal rather than a baroreflex response.[25] These findings explain why desflurane increased HR, whereas isoflurane tended to increase HR, although the difference was not important in this study. Desflurane has more irritating effects on airway membranes than do isoflurane and sevoflurane.[26] Desflurane has been reported to augment laryngeal C-fiber inputs to nucleus tractus solitarii neurons to a greater extent by activating transient receptor potential-A1.[27] These findings explain why desflurane statistically increased HR at high MACs.

The most characteristic finding in this study was that isoflurane statistically increased oral tissue blood flow at a high concentration. Conzen et al[4] compared hepatic, renal, and coronary artery blood flows and circulatory parameters under isoflurane and sevoflurane anesthesia and reported that the rate of decrease in blood flow at high concentrations was less than with isoflurane. This result suggests that different volatile anesthetics produce different effects on regional tissue blood flow. Small vessels have been reported to be affected more readily by volatile anesthetics than large vessels.[5] Previous research has suggested that desflurane exhibits a less potent vasodilatory effect than sevoflurane[19] and that sevoflurane exhibits a less potent vasodilatory effect than isoflurane.[5] These results explain why oral tissue blood flow showed the largest increase in group Iso in the present study.

Cerebral blood flow increases as the concentration of volatile anesthetic increases.[28-30] One study has reported that the cerebrovascular dilatory effect of desflurane is greater than that of sevoflurane or isoflurane.[31] In contrast, in the present study, oral tissue blood flow increased as the concentration increased, although there was little change in CCBF. This result suggests the existence of tissues other than those measured in this study supplied by the common carotid artery where blood flow decreases. Isoflurane has been reported to suppress vasodilation in the submandibular gland through a γ-aminobutyric acidergic mechanism.[32] This blood flow decrease in some oral tissues could be involved in the redistribution of blood flow in the oral region. The blood flow results observed in this study showed trends similar to those of previous studies on hepatic, renal, and coronary artery blood flows.[4,5,19] These results suggest

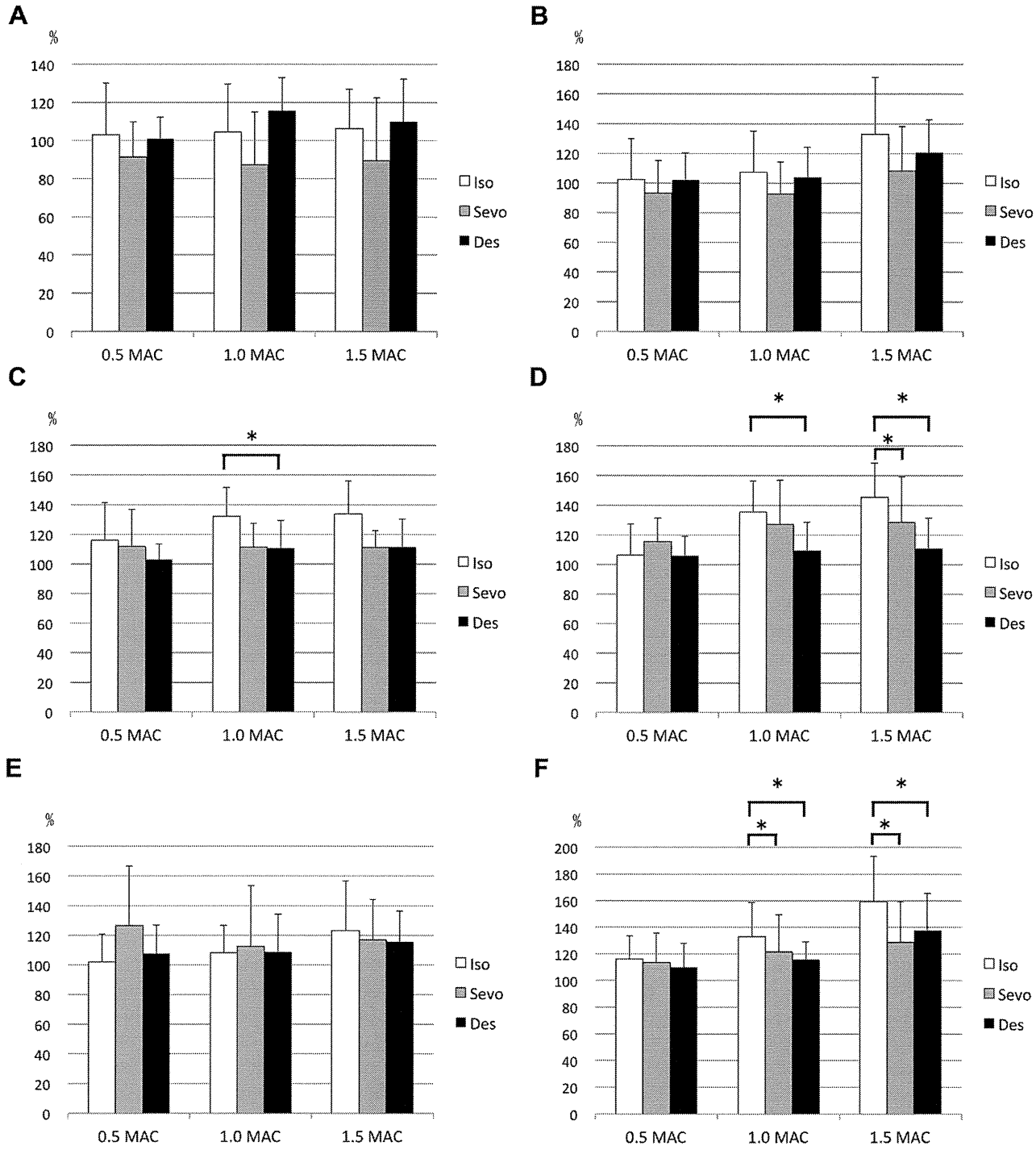

FIGURE 2. Graphs present comparisons among volatile anesthetics at the same MACs. *A*, Percentage of changes from control in CCBF. *B*, Percentage of changes from control in TBF. *C*, Percentage of changes from control in BBF. *D*, Percentage of changes from control in MBF. *E*, Percentage of changes from control in UBF. *F*, Percentage of changes from control in LBF. $*P < .05$ between 2 groups. BBF, bone marrow blood flow; CCBF, common carotid artery blood flow; DBP, diastolic blood pressure; Des, desflurane; HR, heart rate; Iso, isoflurane; LBF, lower alveolar tissue blood flow; MAC, minimum alveolar concentration; MAP, mean arterial pressure; MBF, masseter muscle blood flow; SBP, systolic blood pressure; Sevo, sevoflurane; TBF, tongue mucosal blood flow; UBF, upper alveolar tissue blood flow.

Okamoto, Matsuura, and Ichinohe. Effects of Anesthetics on Oral Blood Flow. J Oral Maxillofac Surg 2015.

that the effect of volatile anesthetics on oral tissue blood flow is similar to that on larger blood vessels in other parts of the body. However, further investigations are needed, because of the possibility that blood flow is redistributed in various tissues in the orofacial region.

Özarslan et al[17] compared sevoflurane with isoflurane in patients undergoing nasal septal surgery and

reported that blood loss was less in the sevoflurane group. Rossi et al[33] compared blood loss during orthognathic surgery using desflurane or sevoflurane and reported less blood loss with desflurane. However, a simple comparison cannot be made with these studies, because fentanyl or remifentanil also was used, and there could be some interactions between volatile anesthetics and opioid analgesics. For this reason, there are some problems with considering the application of the results in this study to the clinical setting. According to Koshika et al,[8] remifentanil produces a concentration-dependent decrease in oral tissue blood flow and decreases oral tissue blood flow more in combination with sevoflurane than with propofol. Therefore, further studies are needed to investigate the drug interactions that can occur when a combination of drugs is used in general anesthesia.

In this study, 10 rabbits were enrolled in each group. This was because power analysis of the results of preliminary experiments suggested that 10 to 11 rabbits in each group were adequate to detect the difference of BBF change, the most important variable for orthognathic surgery, at 1 MAC among the 3 anesthetics (α error, 0.05; β error, 0.2). Accordingly, the present results indicated that the power was almost 0.8.

In conclusion, each volatile anesthetic produced unique effects on regional tissue blood flow and circulatory parameters. The decrease in blood pressure by desflurane was less than that by isoflurane and sevoflurane. Desflurane showed the smallest effects on oral tissue blood flow.

References

1. Dong Y, Teoh HL, Chan BP, et al: Changes in cerebral hemodynamic and cognitive parameters after external carotid-internal carotid bypass surgery in patients with severe steno-occlusive disease: A pilot study. J Neurol Sci 322:112, 2012
2. Ogawa K, Yamamoto M, Mizumoto K, et al: Volatile anaesthetics attenuate hypocapnia-induced constriction in isolated dog cerebral arteries. Can J Anaesth 44:426, 1997
3. Luginbuehl IA, Fredrickson MJ, Karsli C, et al: Cerebral blood flow velocity in children anaesthetized with desflurane. Paediatr Anaesth 13:496, 2003
4. Conzen PF, Vollmar B, Habazettl H, et al: Systemic and regional hemodynamics of isoflurane and sevoflurane in rats. Anesth Analg 74:79, 1992
5. Nakamura K, Toda H, Hatano Y, et al: Comparison of the direct effects of sevoflurane, isoflurane and halothane on isolated canine coronary arteries. Can J Anaesth 40:257, 1993
6. Lischke V, Busse R, Hecker M: Inhalation anesthetics inhibit the release of endothelium-derived hyperpolarizing factor in the rabbit carotid artery. Anesthesiology 83:574, 1995
7. Handa M, Ichinohe T, Kaneko Y: Changes in partial pressure of arterial carbon dioxide induces redistribution of oral tissue blood flow in the rabbit. J Oral Maxillofac Surg 66: 1820, 2008
8. Koshika K, Ichinohe T, Kaneko Y: Dose-dependent remifentanil decreases oral tissue blood flow during sevoflurane and propofol anesthesia in rabbits. J Oral Maxillofac Surg 69: 2128, 2011
9. Sazuka S, Matsuura N, Ichinohe T: Dexmedetomidine dose dependently decreases oral tissue blood flow during sevoflurane and propofol anesthesia in rabbits. J Oral Maxillofac Surg 70: 1808, 2012
10. Ichinohe T, Homma Y, Kaneko Y: Mucosal blood flow during various intravenous and inhalational anesthetics in the rabbit. Oral Surg Oral Med Oral Pathol Oral Radiol Endod 85:268, 1998
11. Terakawa Y, Ichinohe T, Kaneko Y: Rocuronium and vecuronium do not affect mandibular bone marrow and masseter muscular blood flow in rabbits. J Oral Maxillofac Surg 68: 15, 2010
12. Kemmochi M, Ichinohe T, Kaneko Y: Remifentanil decreases mandibular bone marrow blood flow during propofol or sevoflurane anesthesia in rabbits. J Oral Maxillofac Surg 67:1245, 2009
13. Nishizawa S, Ichinohe T, Kaneko Y: Tissue blood flow reductions induced by remifentanil in rabbits and the effect of naloxone and phentolamine on these changes. J Oral Maxillofac Surg 70: 797, 2012
14. Drummond JC: MAC for halothane, enflurane, and isoflurane in the New Zealand White rabbit: And a test for the validity of MAC determinations. Anesthesiology 62:336, 1985
15. Scheller MS, Saidman LJ, Partridge BL: MAC of sevoflurane in humans and the New Zealand White rabbit. Can J Anaesth 35:153, 1988
16. Doorley BM, Waters SJ, Terrell RC, et al: MAC of I-653 in beagle dogs and New Zealand White rabbits. Anesthesiology 69:89, 1988
17. Özarslan NG, Ayhan B, Kanbak M, et al: Comparison of the effects of sevoflurane, isoflurane, and desflurane on microcirculation in coronary artery bypass graft surgery. J Cardiothorac Vasc Anesth 26:791, 2012
18. Scheeren TW, Schwarte LA, Arndt JO: Metabolic regulation of cardiac output during inhalation anaesthesia in dogs. Acta Anaesthesiol Scand 43:421, 1999
19. Park KW, Dai HB, Lowenstein E, et al: Effect of sevoflurane and desflurane on the myogenic constriction and flow-induced dilation in rat coronary arterioles. Anesthesiology 90:1422, 1999
20. Blaudszun G, Morel DR: Superiority of desflurane over sevoflurane and isoflurane in the presence of pressure-overload right ventricle hypertrophy in rats. Anesthesiology 117: 1051, 2012
21. Picker O, Schwarte LA, Schindler AW, et al: Desflurane increases heart rate independent of sympathetic activity in dogs. Eur J Anaesthesiol 20:945, 2003
22. Toader E, Cividjian A, Quintin L: Isoflurane suppresses central cardiac parasympathetic activity in rats: A pilot study. Minerva Anestesiol 77:142, 2011
23. Picker O, Scheeren TW, Arndt JO: Inhalation anaesthetics increase heart rate by decreasing cardiac vagal activity in dogs. Br J Anaesth 87:748, 2001
24. Rampil IJ, Weiskopf RB, Brown JG, et al: I653 and isoflurane produce similar dose-related changes in the electroencephalogram of pigs. Anesthesiology 69:298, 1988
25. Marano G, Grigioni M, Tiburzi F, et al: Effects of isoflurane on cardiovascular system and sympathovagal balance in New Zealand White rabbits. J Cardiovasc Pharmacol 28:513, 1996
26. TerRiet MF, DeSouza GJ, Jacobs JS, et al: Which is most pungent: Isoflurane, sevoflurane or desflurane? Br J Anaesth 85: 305, 2000
27. Mutoh T, Taki Y, Tsubone H: Desflurane but not sevoflurane augments laryngeal C-fiber inputs to nucleus tractus solitarii neurons by activating transient receptor potential-A1. Life Sci 92: 821, 2013
28. Young WL: Effects of desflurane on the central nervous system. Anesth Analg 75:S32, 1992
29. Van Aken H, Van Hemelrijck J: Influence of anesthesia on cerebral blood flow and cerebral metabolism: An overview. Agressologie 32:303, 1991
30. Hansen TD, Warner DS, Todd MM, et al: The role of cerebral metabolism in determining the local cerebral blood flow effects of volatile anesthetics: Evidence for persistent

flow-metabolism coupling. J Cereb Blood Flow Metab 9:323, 1989
31. Holmström A, Rosén I, Akeson J: Desflurane results in higher cerebral blood flow than sevoflurane or isoflurane at hypocapnia in pigs. Acta Anaesthesiol Scand 48:400, 2004
32. Mizuta K, Mizuta F, Takahashi M, et al: Effects of isoflurane on parasympathetic vasodilatation in the rat submandibular gland. J Dent Res 85:379, 2006
33. Rossi A, Falzetti G, Donati A, et al: Desflurane versus sevoflurane to reduce blood loss in maxillofacial surgery. J Oral Maxillofac Surg 68:1007, 2010

Tissue Blood Flow During Remifentanil Infusion With Carbon Dioxide Loading

Hiroaki Kanbe, DDS, PhD,* Nobuyuki Matsuura, DDS, PhD,† Masataka Kasahara, DDS, PhD,† Tatsuya Ichinohe, DDS, PhD‡

*Assistant Professor, †Senior Assistant Professor, and ‡Professor, Department of Dental Anesthesiology, Tokyo Dental College, Chiba, Japan

The aim of this study was to investigate the effect of changes in end-tidal carbon dioxide tension ($ETCO_2$) during remifentanil (Remi) infusion on oral tissue blood flow in rabbits. Eight male tracheotomized Japan White rabbits were anesthetized with sevoflurane under mechanical ventilation. The infusion rate of Remi was 0.4 μg/kg/min. Carbon dioxide was added to the inspired gas to change the inspired CO_2 tension to prevent changes in the ventilating condition. Observed variables were systolic blood pressure (SBP), diastolic blood pressure (DBP), mean arterial pressure (MAP), heart rate (HR), common carotid artery blood flow (CCBF), tongue mucosal blood flow (TBF), mandibular bone marrow tissue blood flow (BBF), masseter muscle tissue blood flow (MBF), upper alveolar tissue blood flow (UBF), and lower alveolar tissue blood flow (LBF). The CCBF, TBF, BBF, UBF, and LBF values were increased, while MBF was decreased, under hypercapnia, and vice versa. The BBF, UBF, and LBF values were increased, while the MBF value was decreased, under hypercapnia during Remi infusion, and vice versa. The BBF, MBF, UBF, and LBF values, but not the CCBF and TBF values, changed along with $ETCO_2$ changes during Remi infusion.

Key Words: Remifentanil; Oral tissue blood flow; Hypercapnia; Hypocapnia; End-tidal carbon dioxide

The oral region comprises mucosa and bone marrow, which include abundant vessels. Control of bleeding during oral and maxillofacial surgery is therefore important to establish a clear surgical field, to avoid blood transfusion, and to secure rapid postoperative recovery. Deliberate hypotension is a conventional method to reduce tissue blood flow during oral and maxillofacial surgery.[1–4] However, some reports pointed out that this technique may cause brain injury and other complications.[5,6]

Accordingly, we have researched another approach to control tissue blood flow in the oral region during general anesthesia. Handa et al[7] reported that hypercapnia increases common carotid artery blood flow (CCBF) and mandibular bone marrow tissue blood flow (BBF), while it decreases masseter muscle tissue blood flow (MBF). Kemmochi et al[8] reported that remifentanil (Remi) decreases CCBF and BBF without a substantial reduction of blood pressure. Koshika et al[9] reported that Remi decreases tongue mucosal blood flow (TBF), BBF, MBF, upper alveolar tissue blood flow (UBF), and lower alveolar tissue blood flow (LBF) in a dose-dependent manner and that a Remi infusion at a rate of 0.2 μg/kg/min decreases oral tissue blood flow without a substantial reduction of heart rate (HR) and blood pressure. Based on these findings, we suppose that changes in tissue blood flow may be modified by changes in arterial carbon dioxide level during Remi infusion. However, there has been no report that investigates the effect of a combination of Remi infusion and the change in arterial carbon dioxide level on oral tissue blood flow. In this study, therefore, we investigated the effect of changes in

Received November 16, 2013; accepted for publication December 20, 2014.

Address correspondence to Dr Hiroaki Kanbe, Department of Dental Anesthesiology, Tokyo Dental College, 1-2-2, Masago, Mihama-ku, Chiba 261-8502, Japan; kanbehiroaki@tdc.ac.jp.

Anesth Prog 62:51–56 2015

ISSN 0003-3006/15
SSDI 0003-3006(15)

end-tidal carbon dioxide tension ($ETCO_2$) during Remi infusion on oral tissue blood flow in rabbits.

METHOD

Eight male Japan White rabbits weighing approximately 2.5 kg were used in this study. All animals received humane care in accordance with the Guideline for the Treatment of Experimental Animals approved by Tokyo Dental College, Chiba, Japan (approval no. 232501).

Anesthesia was induced with 3.0% isoflurane (Forane, Abbott Japan, Tokyo, Japan). Tracheostomy was performed using infiltration anesthesia with 0.5 mL of 1% lidocaine hydrochloride solution (Xylocaine, AstraZeneca, Osaka, Japan), and then a 20 Fr pediatric tracheal tube was inserted into the trachea and fixed. Animals were ventilated at a tidal volume of 30 to 50 mL and a respiratory rate of 30 to 40 breaths/min. The $ETCO_2$ was measured with an anesthetic gas monitor (Capnomac Ultima, Datex, Helsinki, Finland) and maintained at 30 mm Hg. Intravenous indwelling catheters were placed in the right femoral artery and the left posterior auricular marginal vein. These were used for arterial pressure measurement and as a route of fluid infusion and drug administration, respectively. Arterial pressure was continuously recorded with a pressure transducer (P231D, Gould, Oxnard, Calif), and HR was calculated from pressure waveforms. Acetated Ringer solution was infused at a rate of 10 mL/kg/h. Muscular relaxation was induced by an infusion of rocuronium bromide (Eslax, Schering-Plough, Tokyo, Japan) at a rate of 14 μg/kg/min.[10] An incision was performed along the left inferior margin of the mandible without local anesthesia to expose the periosteum of the mandibular body. The periosteum was then detached to expose the surface of the mandibular body. A small hole penetrating into the bone marrow through the cortical bone was performed using a round bur with the diameter of 0.8 mm (ISO 008, Morita, Saitama, Japan). Needle probes of a hydrogen clearance tissue blood flowmeter (UHE-100, Unique Medical, Tokyo, Japan) were inserted into mandibular bone marrow, left masseter muscle, left upper alveolar tissue, and left lower alveolar tissue. The TBF was continuously monitored using a laser Doppler blood flowmeter (AFL21, Advance, Tokyo, Japan). A contact-type probe (type C, Advance) was placed in close contact with the lingual mucosa on the left side. The CCBF was continuously monitored using an ultrasonic blood flowmeter (T108, Transonic, Ithaca, NY). A flow probe (type 3SB, Transonic) was fixed to the left common carotid artery.

Systolic blood pressure (SBP), diastolic blood pressure (DBP), mean arterial pressure (MAP), HR, CCBF, and TBF were continuously recorded on a polygraph (Serise360, NEC San-ei, Tokyo, Japan). The BBF, MBF, UBF, and LBF values were analyzed by a data collection analysis system (UCO, Unique Medical, Tokyo, Japan). The rectal temperature was maintained between 39.0°C and 39.5°C throughout the experiment.

After experimental preparation had been completed, isoflurane inhalation was discontinued and inhalation of sevoflurane (Sevofrane, Maruishi Pharmaceutical, Osaka, Japan) was started. Sevoflurane was administered to maintain the end-tidal concentration at 1.8%, 0.5 minimum alveolar concentration for rabbits.[11] After the cardiorespiratory parameters had been stabilized for at least 1 hour, the control measurements were performed at an $ETCO_2$ level of 30 mm Hg. Carbon dioxide was then added to the inhaled air, and $ETCO_2$ was raised to 40 mm Hg and maintained for 15 minutes to prevent the changes in the ventilating condition. Thereafter, $ETCO_2$ was again raised to 60 mm Hg and maintained for 15 minutes. All parameters were measured at each time point. Inhalation of CO_2 was then stopped, and the animals were kept at rest for approximately 30 minutes. After recovery of blood pressure and HR to control values was confirmed, Remi (Ultiva: Janssen Pharmaceutical, Tokyo, Japan) infusion at a rate of 0.4 μg/kg/min was started. Each parameter was measured 15 minutes after the start of Remi infusion. Thereafter, CO_2 was again added to the inhaled air. $ETCO_2$ was raised to 40 and then 60 mm Hg at 15-minute intervals, and all parameters were observed at each time point. Finally, inhalation of CO_2 was stopped and animals were kept at rest for more than 30 minutes. Observations were concluded after the recovery of blood pressure and HR to control values during Remi infusion was confirmed.

Values are expressed as mean ± standard deviation. One-way repeated measurements analysis of variance followed by the Student-Neuman-Keuls test was used for statistical analyses. A P value less than .05 was considered statistically significant.

RESULTS

The SBP and MAP values were increased along with $ETCO_2$ elevation, although they did not change despite $ETCO_2$ elevation during Remi infusion. The DBP was increased along with $ETCO_2$ elevation, and it was also increased along with $ETCO_2$ elevation during Remi infusion. The HR was decreased along with $ETCO_2$ elevation, and it was also decreased along with $ETCO_2$

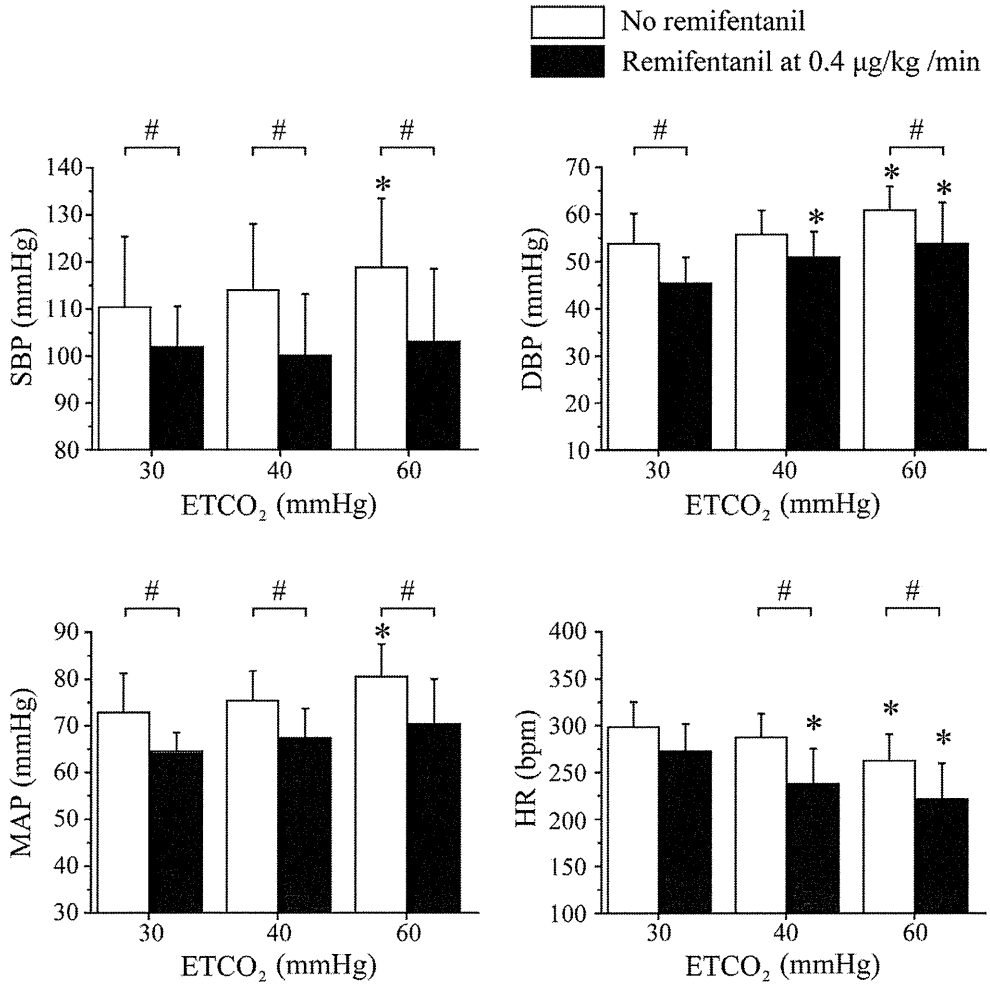

Figure 1. Comparisons of systolic blood pressure (SBP), diastolic blood pressure (DBP), mean arterial pressure (MAP), and heart rate (HR) during remifentanil (Remi) infusion with those during no Remi infusion. All variables were decreased during Remi infusion when compared under identical end-tidal carbon dioxide tension ($ETCO_2$) level. The DBP level was increased and HR was decreased along with $ETCO_2$ elevation during Remi infusion. Data are shown as mean ± SD ($n = 8$). *$P < .05$ versus respective values at $ETCO_2$ 30 mm Hg. #$P < .05$ between two values at the same $ETCO_2$ level.

elevation during Remi infusion. All of these variables were decreased during Remi infusion, when compared under identical $ETCO_2$ level (Figure 1).

The CCBF and TBF values were increased along with $ETCO_2$ elevation, although they did not change despite $ETCO_2$ elevation during Remi infusion. The BBF, UBF, and LBF values were increased along with $ETCO_2$ elevation, and they were also increased along with $ETCO_2$ elevation during Remi infusion. The MBF value was decreased along with $ETCO_2$ elevation, and it was also decreased along with $ETCO_2$ elevation during Remi infusion. All of these variables were decreased during Remi infusion, when compared under identical $ETCO_2$ level (Figure 2).

The CCBF, BBF, UBF, and LBF values at an $ETCO_2$ level of 40 mm Hg without Remi infusion were comparable with those at an $ETCO_2$ level of 60 mm Hg with Remi infusion. In contrast, MBF at an $ETCO_2$ level of 40 mm Hg without Remi infusion was comparable with that at an $ETCO_2$ level of 30 mm Hg with Remi infusion.